



Supporting Information

© Copyright Wiley-VCH Verlag GmbH & Co. KGaA, 69451 Weinheim, 2019

Heteroleptic β -Ketoiminate Zinc Phenoxide Complexes as Efficient Catalysts for the Ring Opening Polymerization of Lactide

Swarup Ghosh, Pascal M. Schäfer, Dennis Dittrich, Christoph Scheiper, Phillip Steiniger, Gerhard Fink, Agnieszka N. Ksiazkiewicz, Alexander Tjaberings, Christoph Wölper, André H. Gröschel, Andrij Pich, Sonja Herres-Pawlis,* and Stephan Schulz* © 2019 The Authors. Published by Wiley-VCH Verlag GmbH & Co. KGaA. This is an open access article under the terms of the Creative Commons Attribution Non-Commercial NoDerivs License, which permits use and distribution in any medium, provided the original work is properly cited, the use is non-commercial and no modifications or adaptations are made.

Content

Fig. S1, S2. ^1H NMR and ^{13}C NMR (CDCl_3 , 25 °C) spectrum of **1**.

Fig. S3, S4. ^1H NMR and ^{13}C NMR (CDCl_3 , 25 °C) spectrum of **2**.

Fig. S5, S6. ^1H NMR and ^{13}C NMR (CDCl_3 , 25 °C) spectrum of **3**.

Fig. S7, S8. ^1H NMR and ^{13}C NMR (CDCl_3 , 25 °C) spectrum of **4**.

Fig. S9. ^1H NMR (300 MHz, CDCl_3 , 25 °C) spectrum of **5**.

Fig. S10. ^1H NMR (300 MHz, Toluene-d₈, 40 °C) spectrum of **5**.

Fig. S11. ^{13}C NMR (300 MHz, CDCl_3 , 25 °C) spectrum of **5**.

Fig. S12. ^1H NMR (300 MHz, CDCl_3 , 25 °C) spectrum of **6**.

Fig. S13. ^1H NMR (300 MHz, Toluene-d₈, 40 °C) spectrum of **6**.

Fig. S14. ^{13}C NMR (300 MHz, CDCl_3 , 25 °C) spectrum of **6**.

Fig. S15. ^1H NMR (300 MHz, CDCl_3 , 25 °C) spectrum of **7**.

Fig. S16. ^1H NMR (300 MHz, Toluene-d₈, 40 °C) spectrum of **7**.

Fig. S17. ^{13}C NMR (300 MHz, CDCl_3 , 25 °C) spectrum of **7**.

Fig. S18. ^1H NMR (300 MHz, CDCl_3 , 25 °C) spectrum of **8**.

Fig. S19. ^1H NMR (300 MHz, Toluene-d₈, 40 °C) spectrum of **8**.

Fig. S20. ^{13}C NMR (300 MHz, CDCl_3 , 25 °C) spectrum of **8**.

Fig. S21-S28. AFT-IR spectrum of **1-8**.

Fig S29-S34. DOSY spectrum of (300 MHz, CDCl_3 , 25 °C) spectrum of **1, 3-6, 8**.

Table S1, S2. Crystal data for complexes **1, 2, 3** and **4** as well as complexes **5, 6, 7** and **8**

Fig S35-39. ORTEP representations of solid-state structures of compounds **3, 4, 6-8**.

Fig S40. Homonuclear decoupled ^1H -NMR spectrum of *rac*-PLA in CDCl_3 (methine H-atom region) obtained by reaction of *rac*-LA and **1** in ratio 200:1 at 25 °C.

Fig S41. Homonuclear decoupled ^1H -NMR spectrum of *rac*-PLA in CDCl_3 (methine H-atom region) obtained by reaction of *rac*-LA and **5** in ratio 200:1 at 25 °C.

Fig S42. Homonuclear decoupled ^1H -NMR spectrum of *L*-PLA in CDCl_3 (methine H-atom region) obtained by reaction of *L*-LA and **1** in ratio 200:1 at 25 °C.

Fig S43. Homonuclear decoupled ^1H -NMR spectrum of *L*-PLA in CDCl_3 (methine H-atom region) obtained by reaction of *L*-LA and **5** in ratio 200:1 at 25 °C.

Fig S44. ^1H -NMR spectrum of *L*-PLA in CDCl_3 from the reaction of *L*-LA and **1** (ratio 50:1, 25 °C, CH_2Cl_2).

Fig S45. ^1H -NMR spectrum of *L*-PLA in CDCl_3 from the reaction of *L*-LA and **5** (ratio 50:1, 25 °C, CH_2Cl_2)

Fig S46. IR spectrum of *L*-PLA obtained by reaction of *L*-LA and **5** in ratio 50:1 at 25 °C in CH_2Cl_2 .

Fig S47. MALDI-TOF spectrum of *L*-PLA obtained by reaction of *L*-LA and **1** in ratio 50:1 at 25 °C in CH_2Cl_2 (Bruker ultrafleXtreme; Polymerix – Sierra Analytics; Aachen).

Table S3 Polymerization data of *L*-LA using catalyst **1** on the variations of M_n with $[M]_0/[C]_0$ ratio in CH_2Cl_2 at 25 °C under argon atmosphere.

Table S4 NBO analysis of the Zn atom and oxygen atom of the phenoxide group for **1-8**.

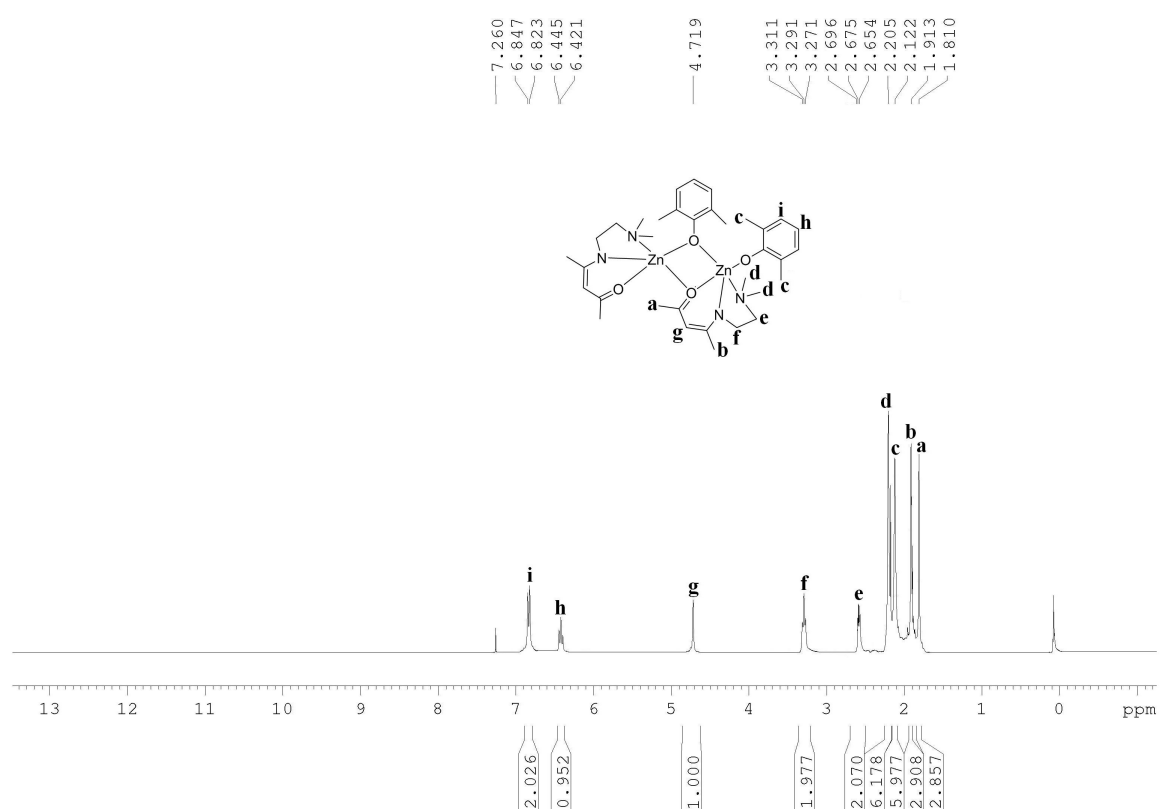


Fig. S1. ^1H NMR (300 MHz, CDCl_3 , 25 °C) spectrum of **1**

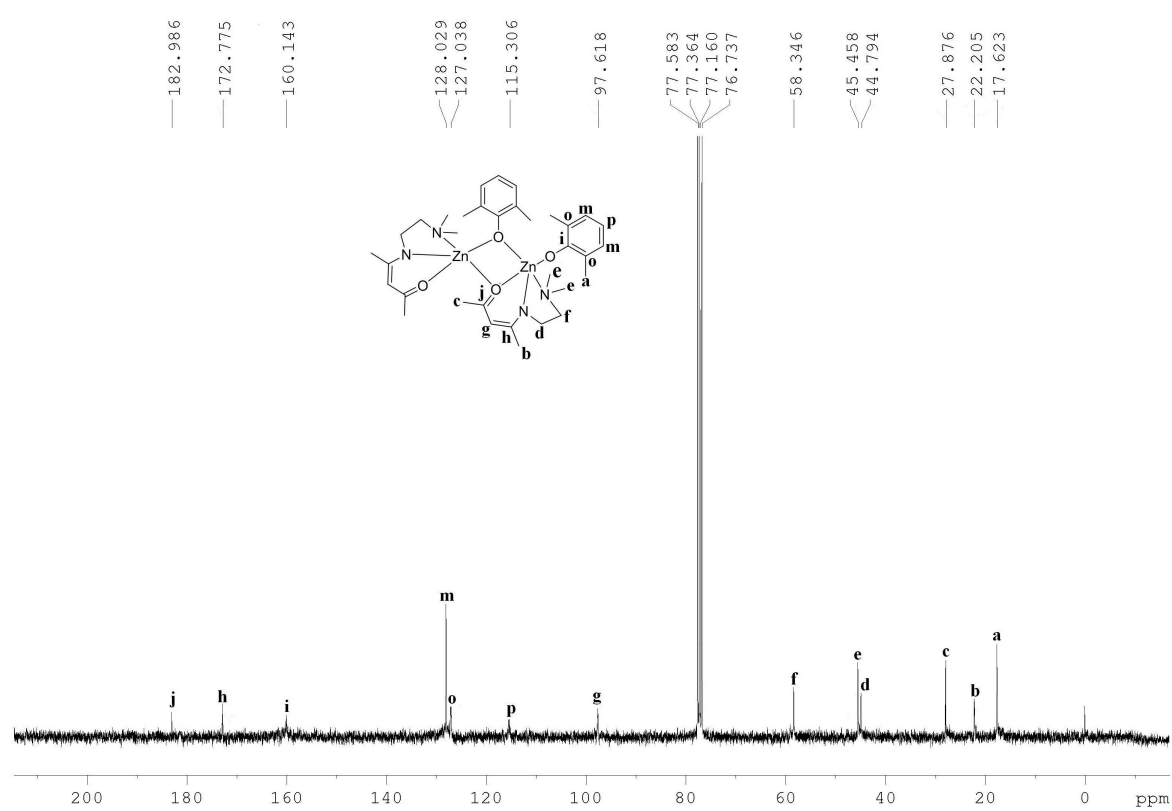


Fig. S2. ^{13}C NMR (75 MHz, CDCl_3 , 25 °C) spectrum of **1**

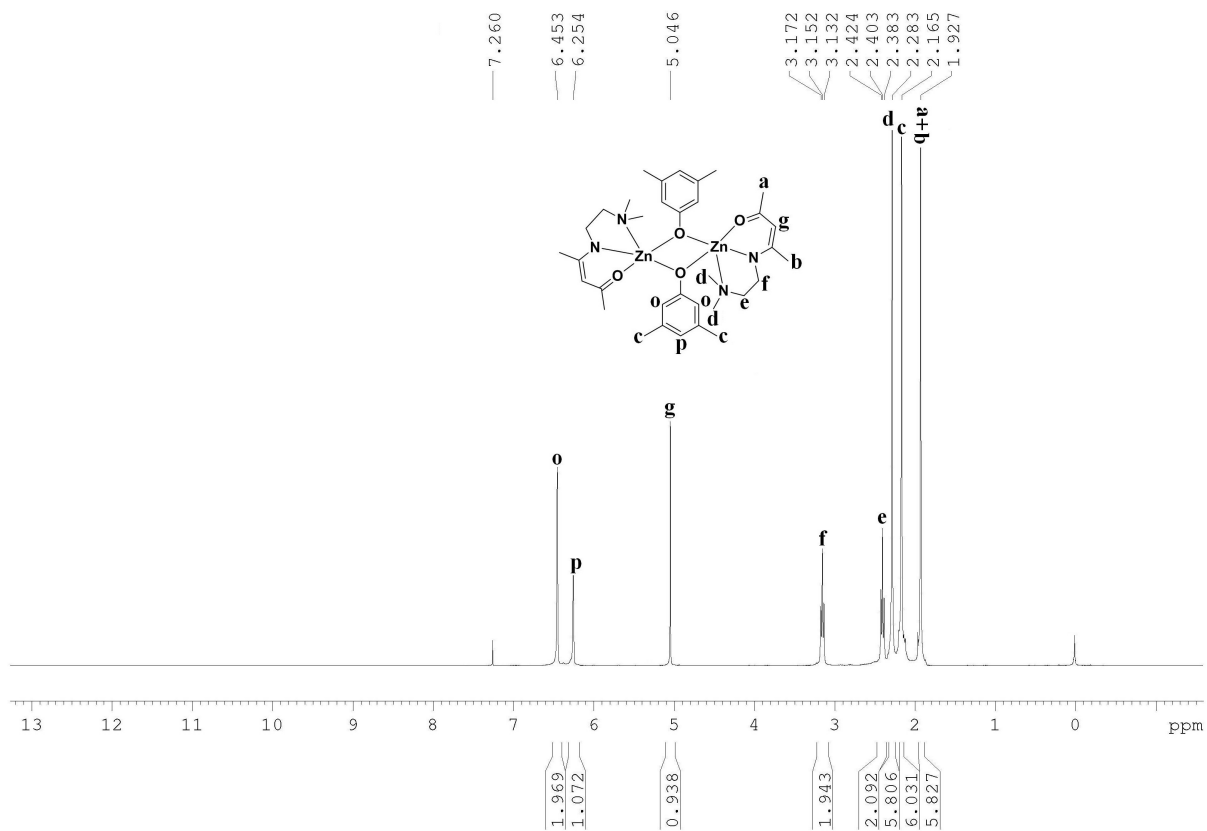


Fig. S3. ¹H NMR (300 MHz, CDCl₃, 25 °C) spectrum of 2

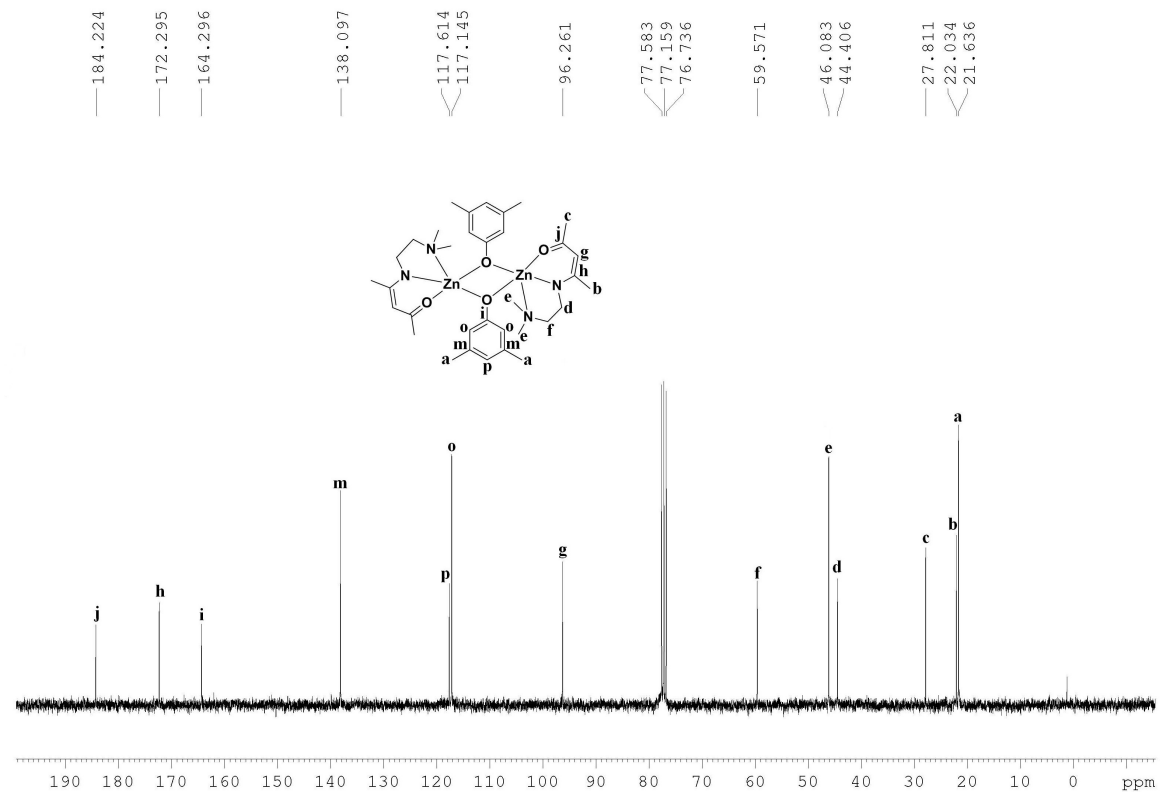


Fig. S4. ¹³C NMR (75 MHz, CDCl₃, 25 °C) spectrum of 2

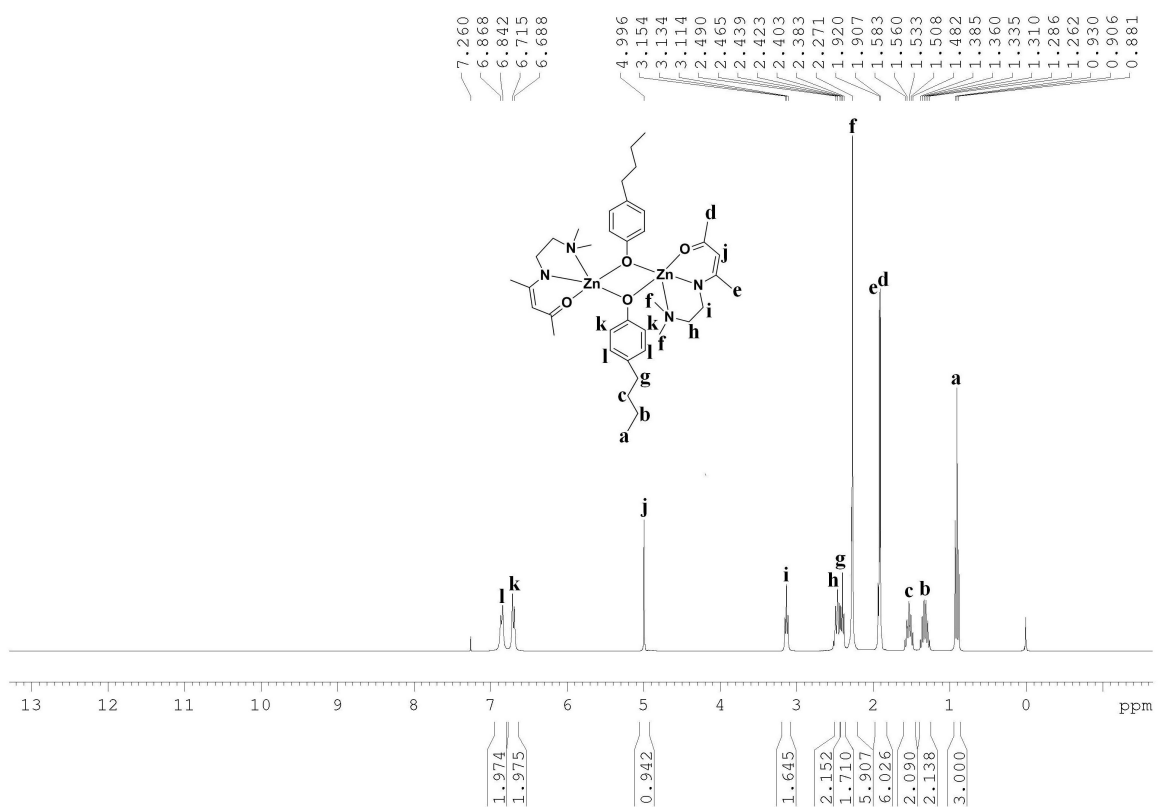


Fig. S5. ^1H NMR (300 MHz, CDCl_3 , 25 °C) spectrum of **3**

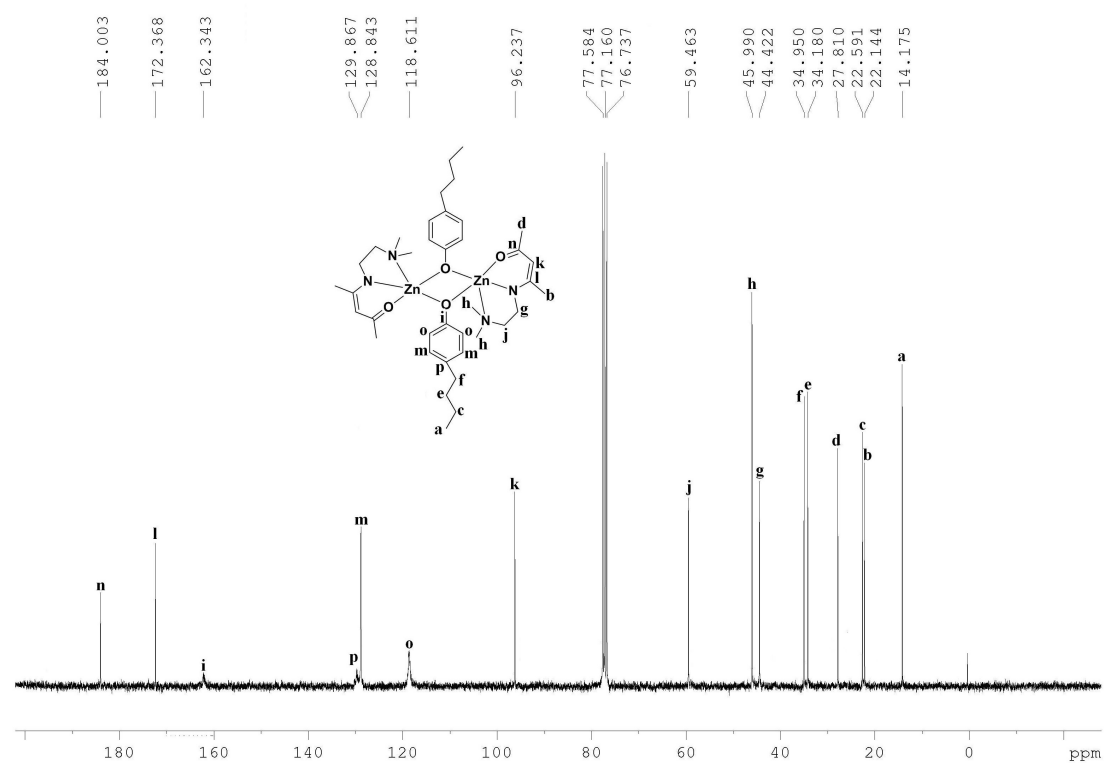


Fig. S6. ^{13}C NMR (75 MHz, CDCl_3 , 25 °C) spectrum of **3**

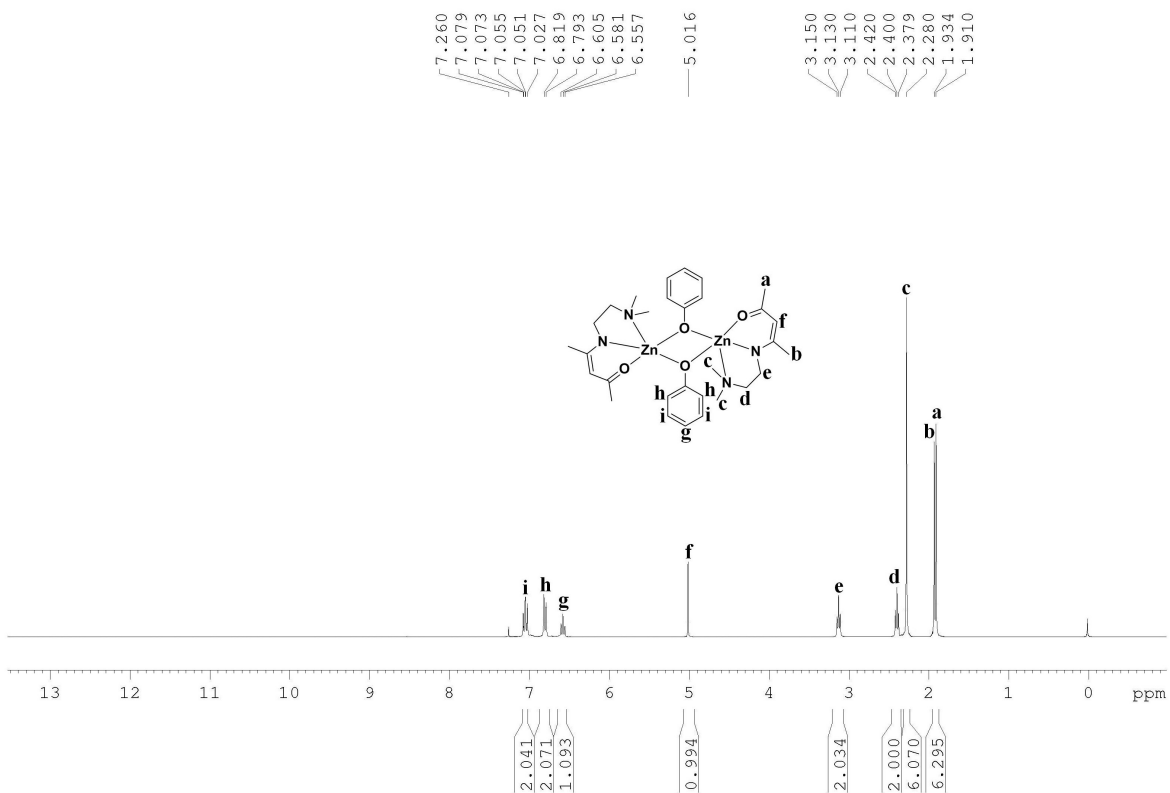


Fig. S7. ^1H NMR (300 MHz, CDCl_3 , 25 °C) spectrum of 4

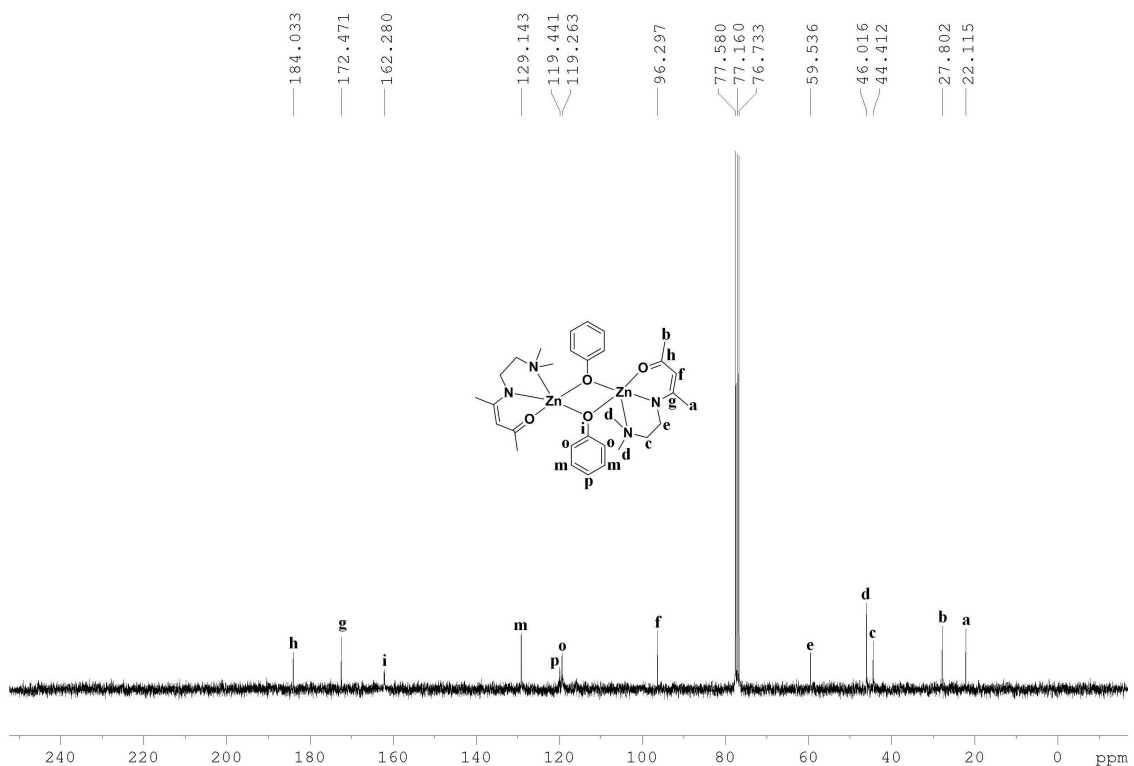


Fig. S8. ^{13}C NMR (75 MHz, CDCl_3 , 25 °C) spectrum of 4

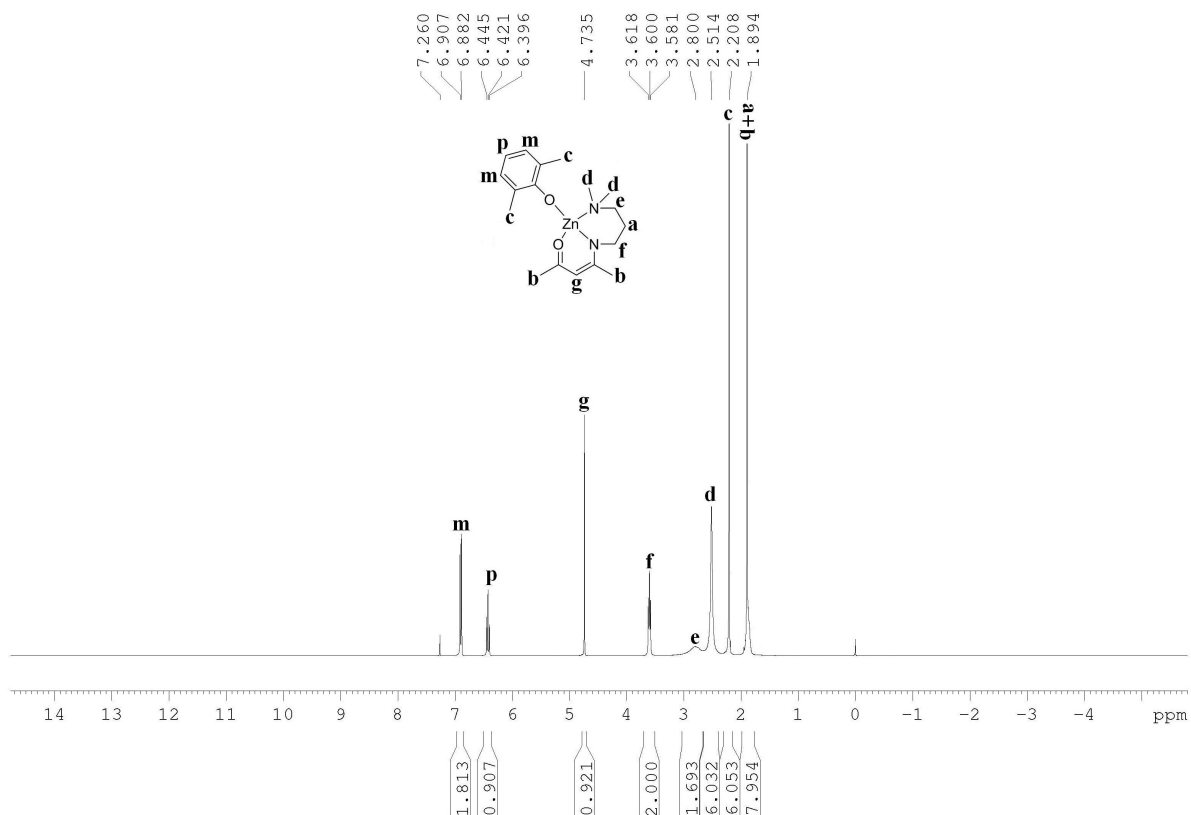


Fig. S9. ^1H NMR (300 MHz, CDCl_3 , 25 °C) spectrum of **5**

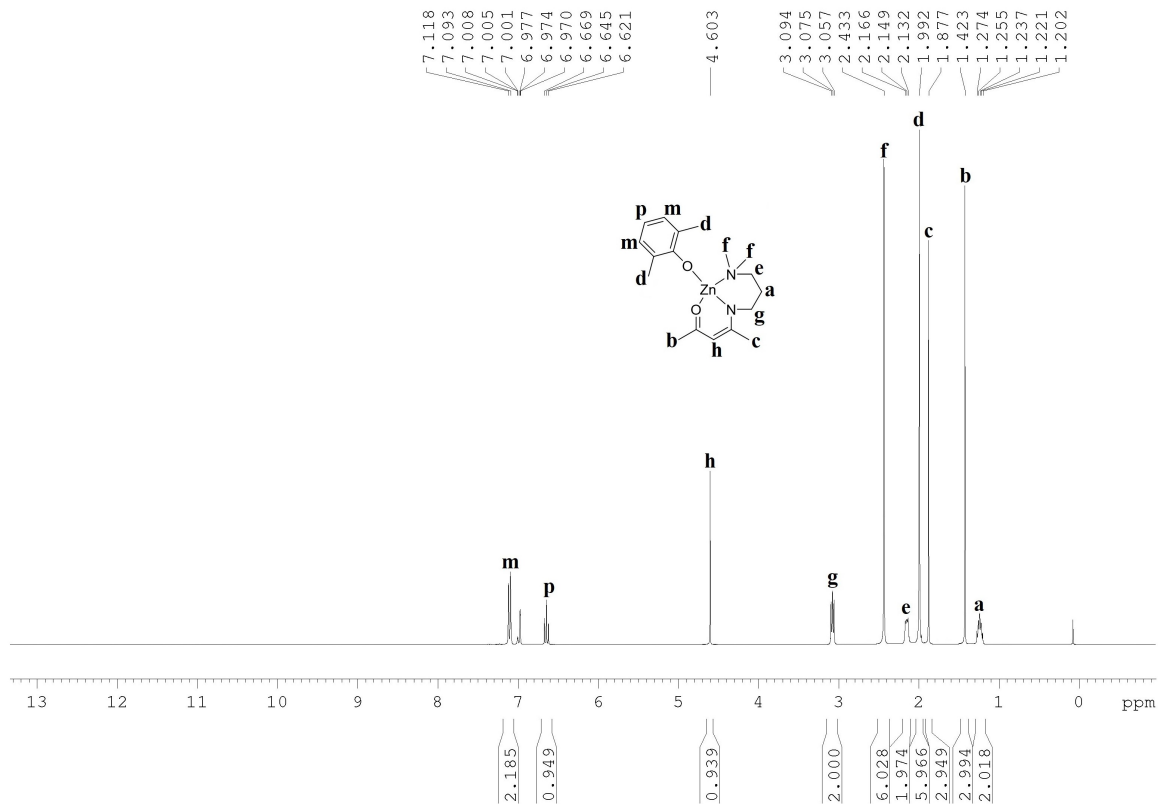


Fig. S10. ^1H NMR (300 MHz, Toluene-d8, 40 °C) spectrum of **5**

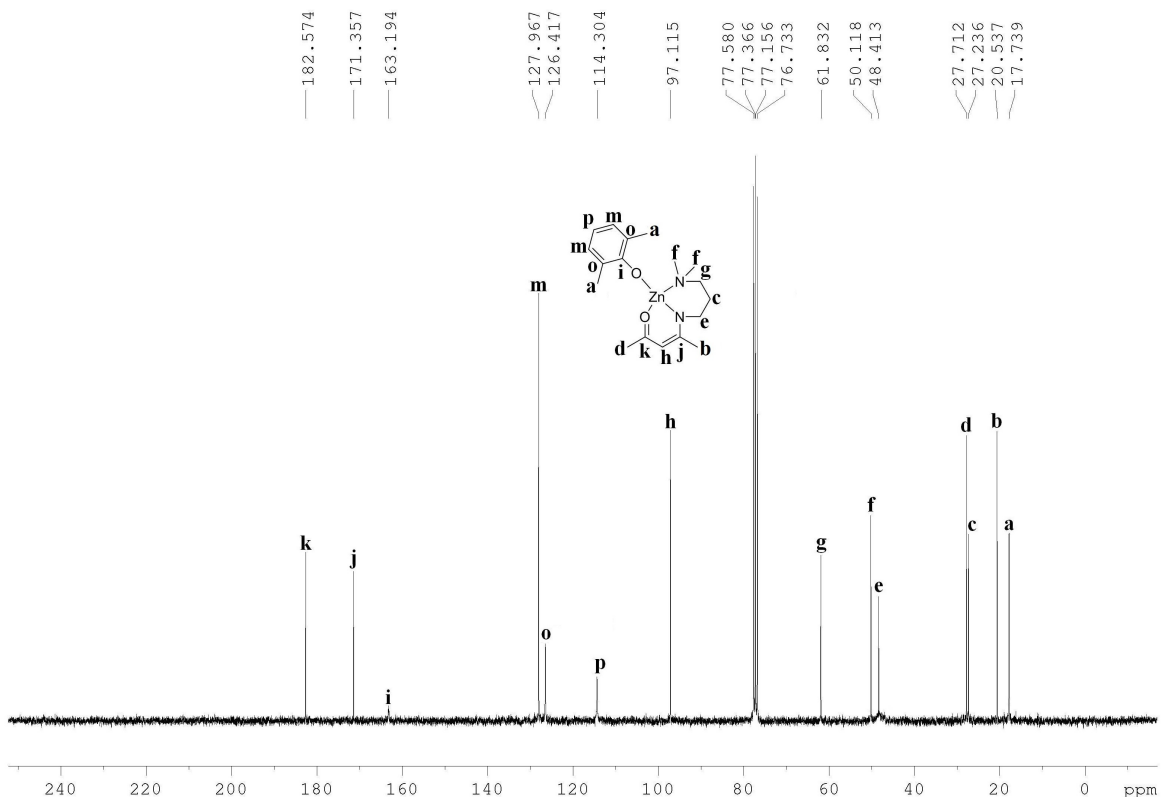


Fig. S11. ^{13}C NMR (300 MHz, CDCl_3 , 25 °C) spectrum of **5**

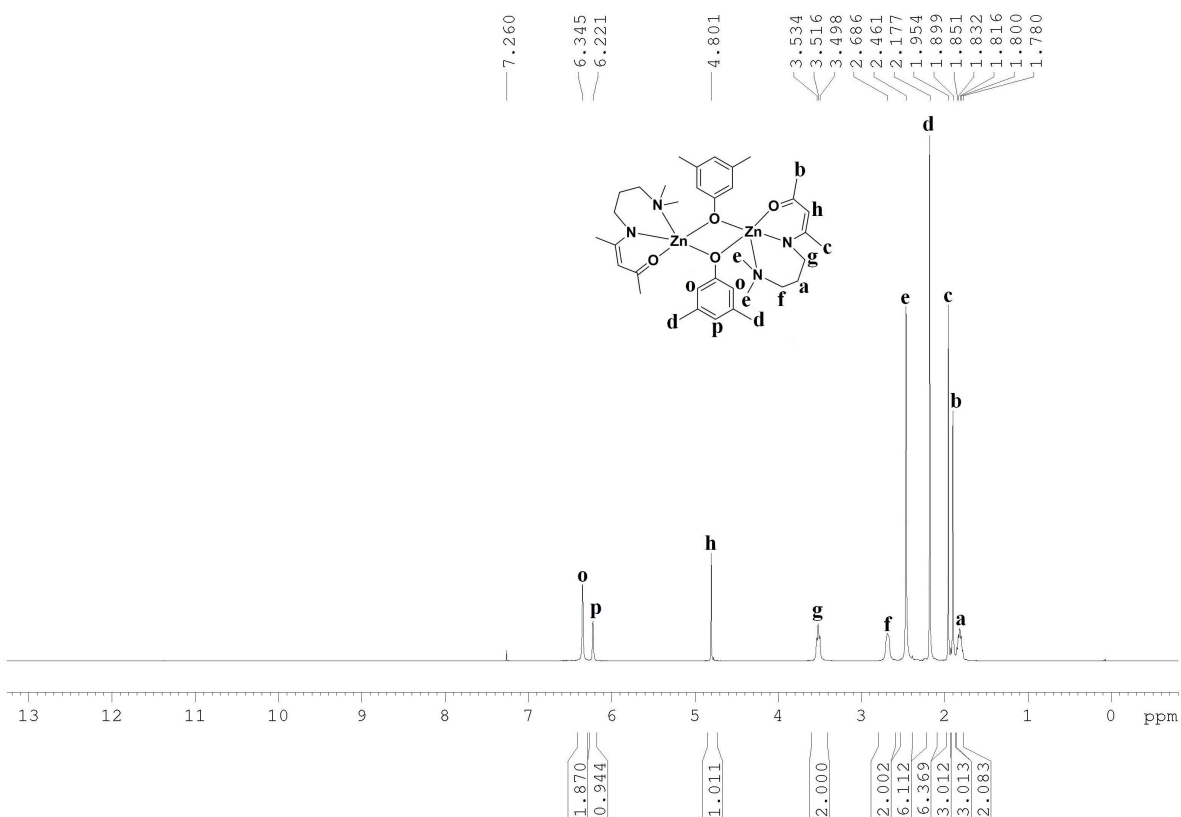


Fig. S12. ^1H NMR (300 MHz, CDCl_3 , 25 °C) spectrum of **6**

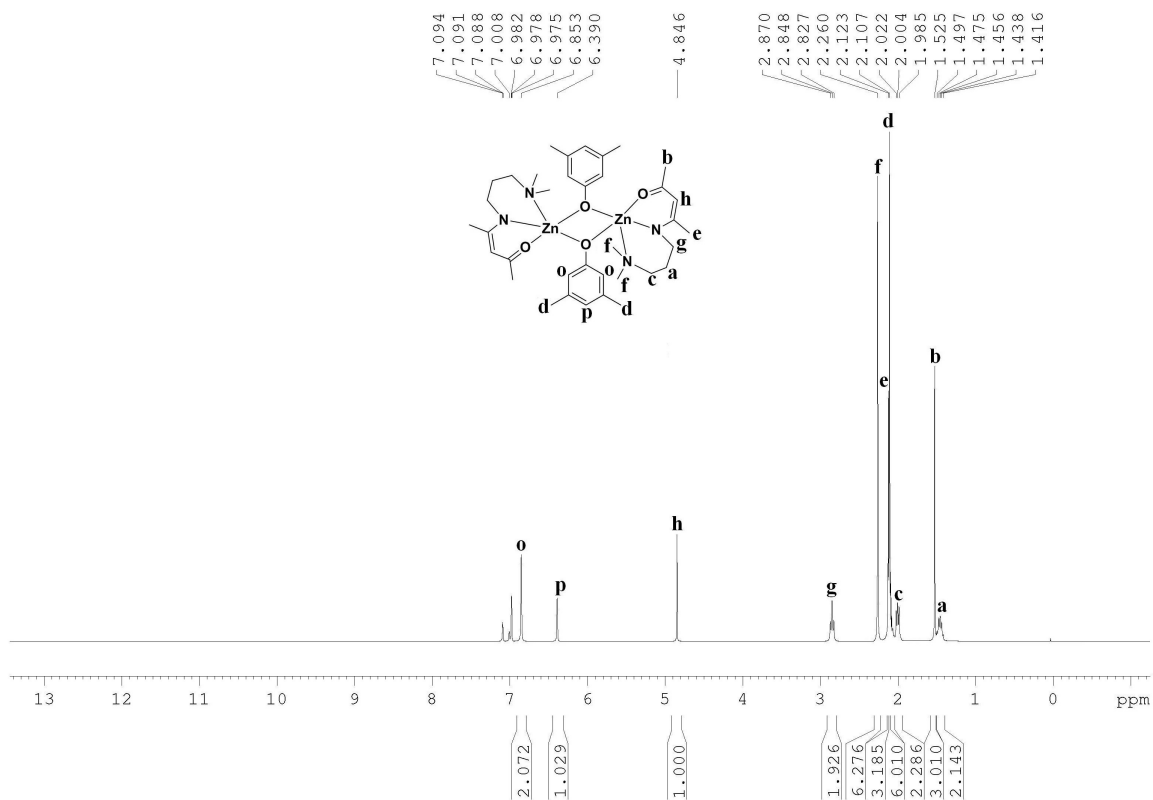


Fig. S13. ^1H NMR (300 MHz, Toluene-d8, 40 °C) spectrum of **6**

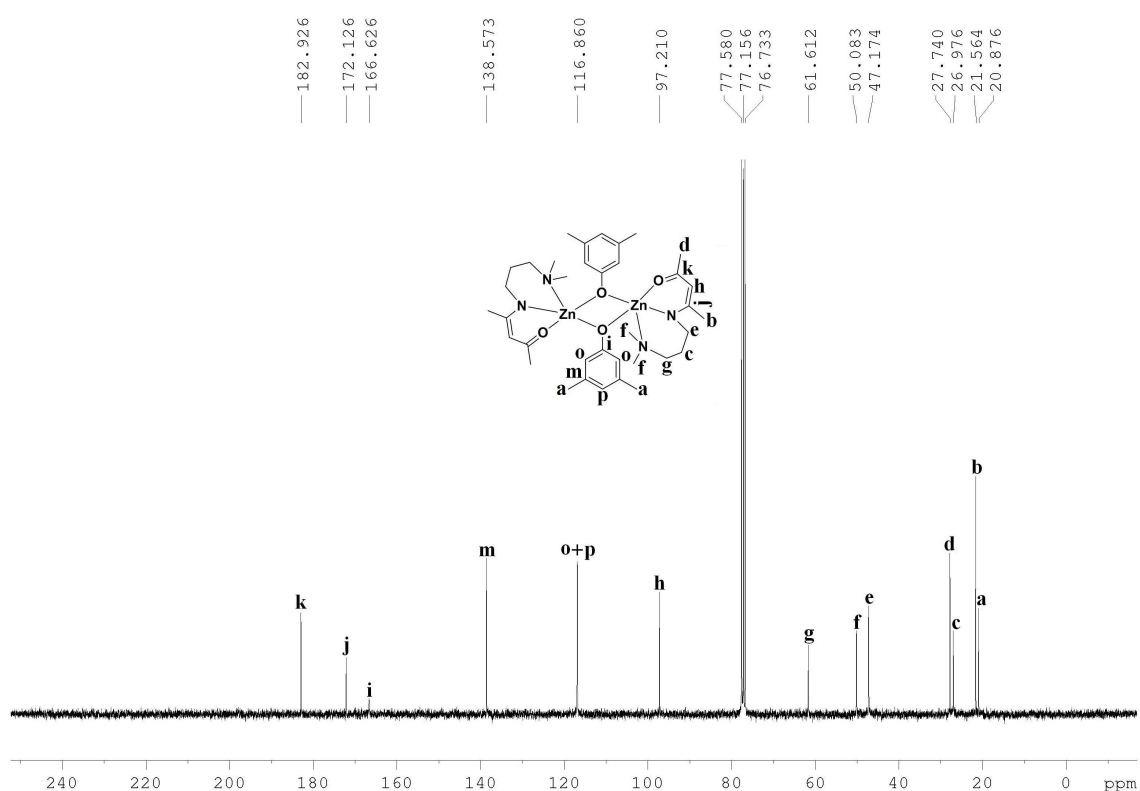


Fig. S14. ^{13}C NMR (300 MHz, CDCl_3 , 25 °C) spectrum of **6**

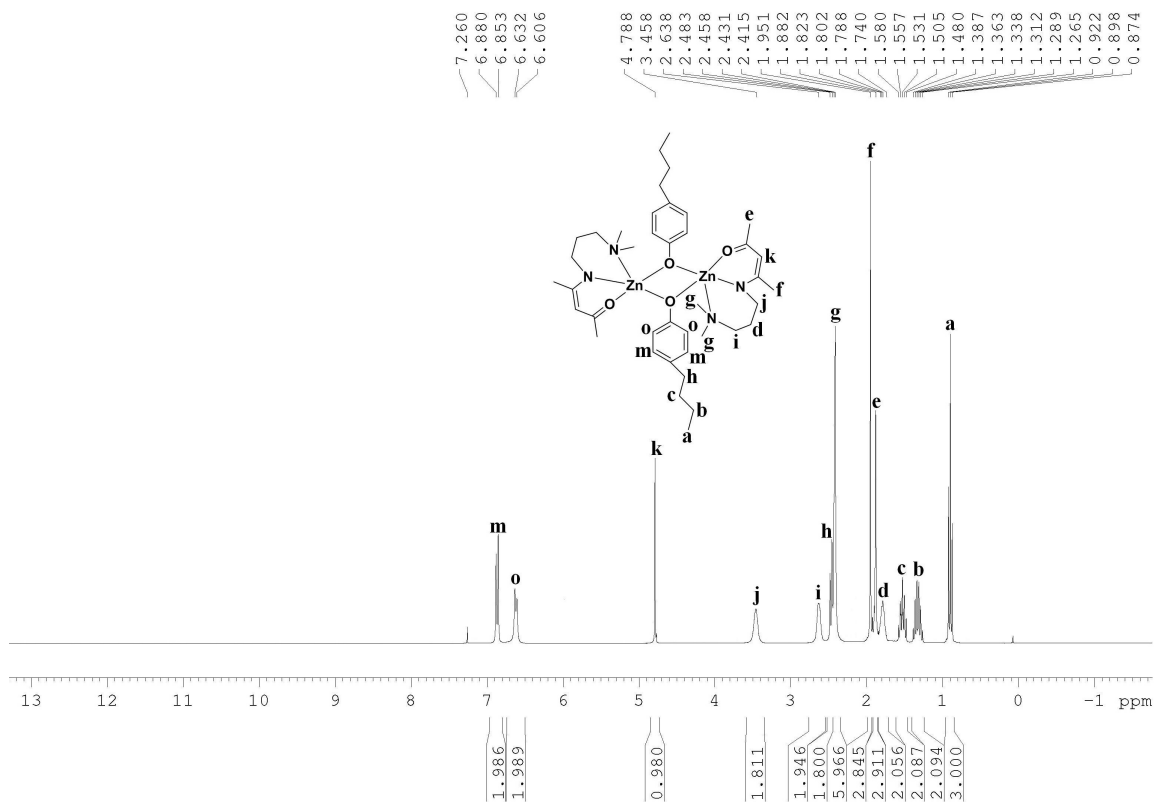


Fig. S15. ^1H NMR (300 MHz, CDCl_3 , 25 °C) spectrum of **7**

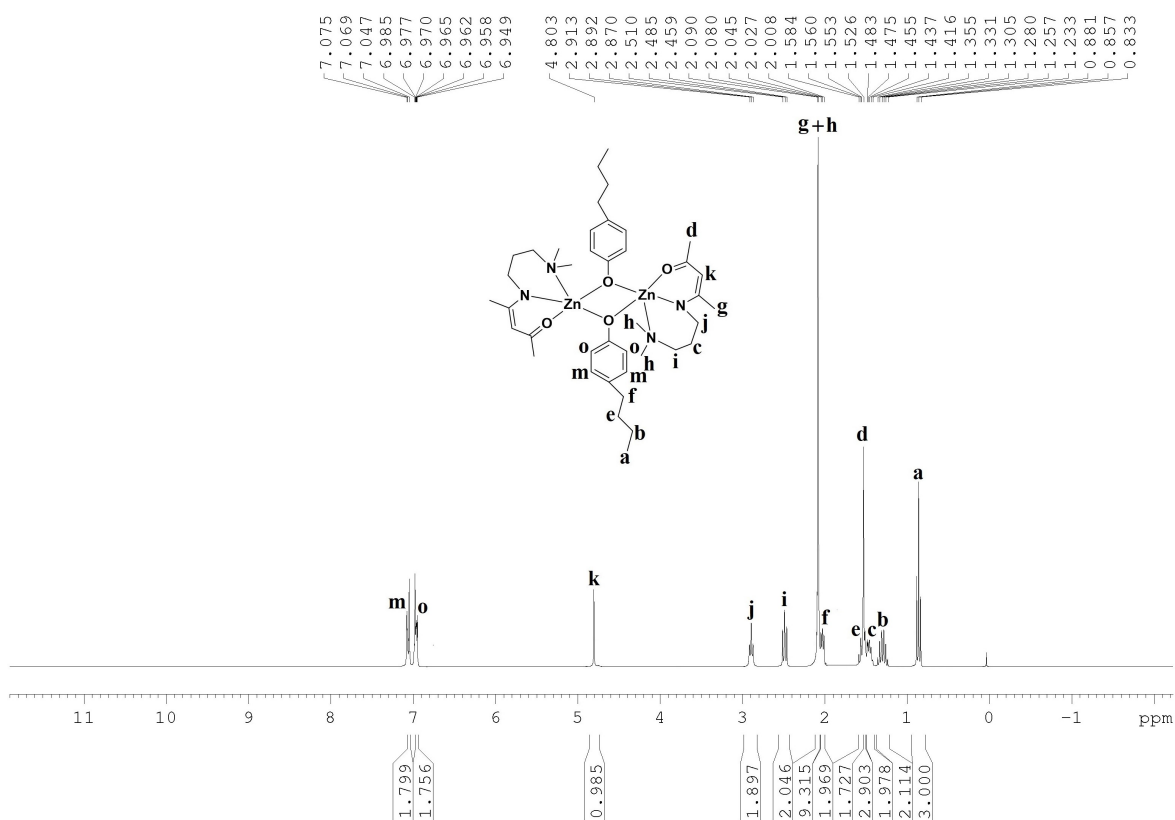


Fig. S16. ^1H NMR (300 MHz, Toluene-d8 , 40 °C) spectrum of **7**

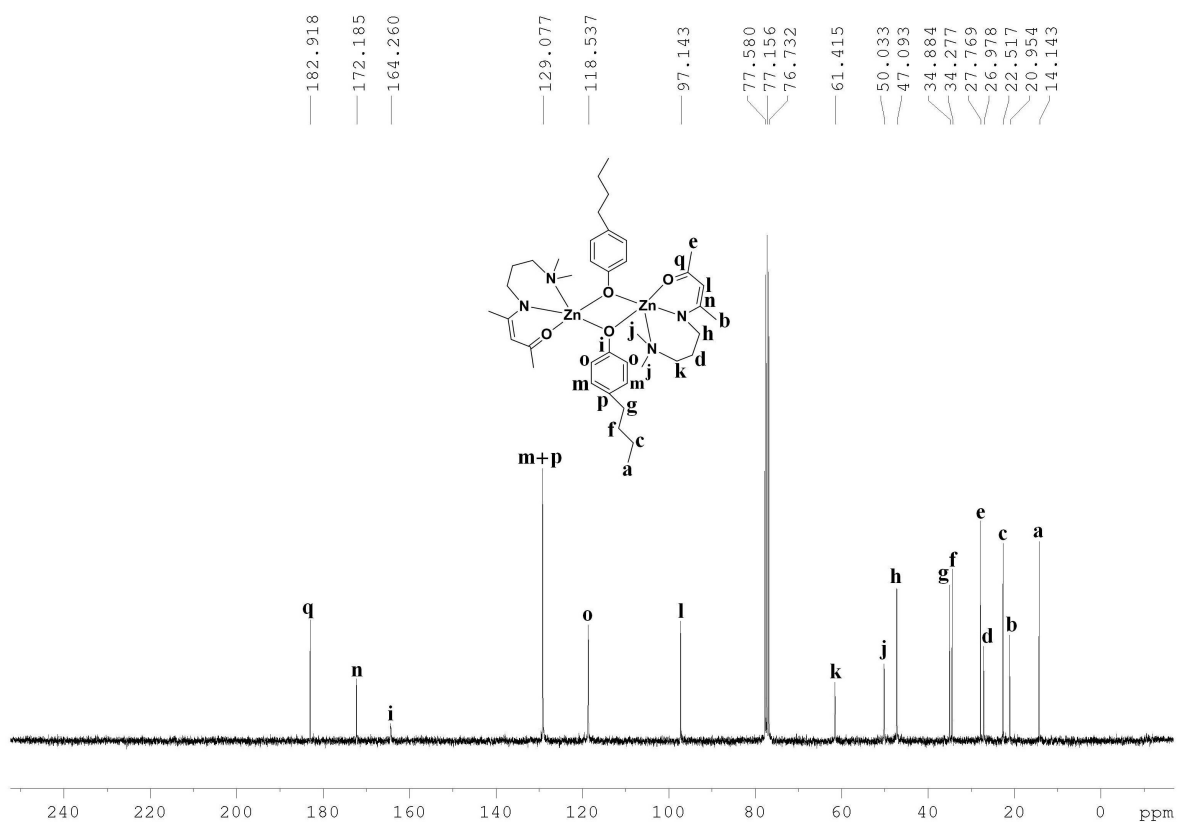


Fig. S17. ^{13}C NMR (300 MHz, CDCl_3 , 25 °C) spectrum of 7

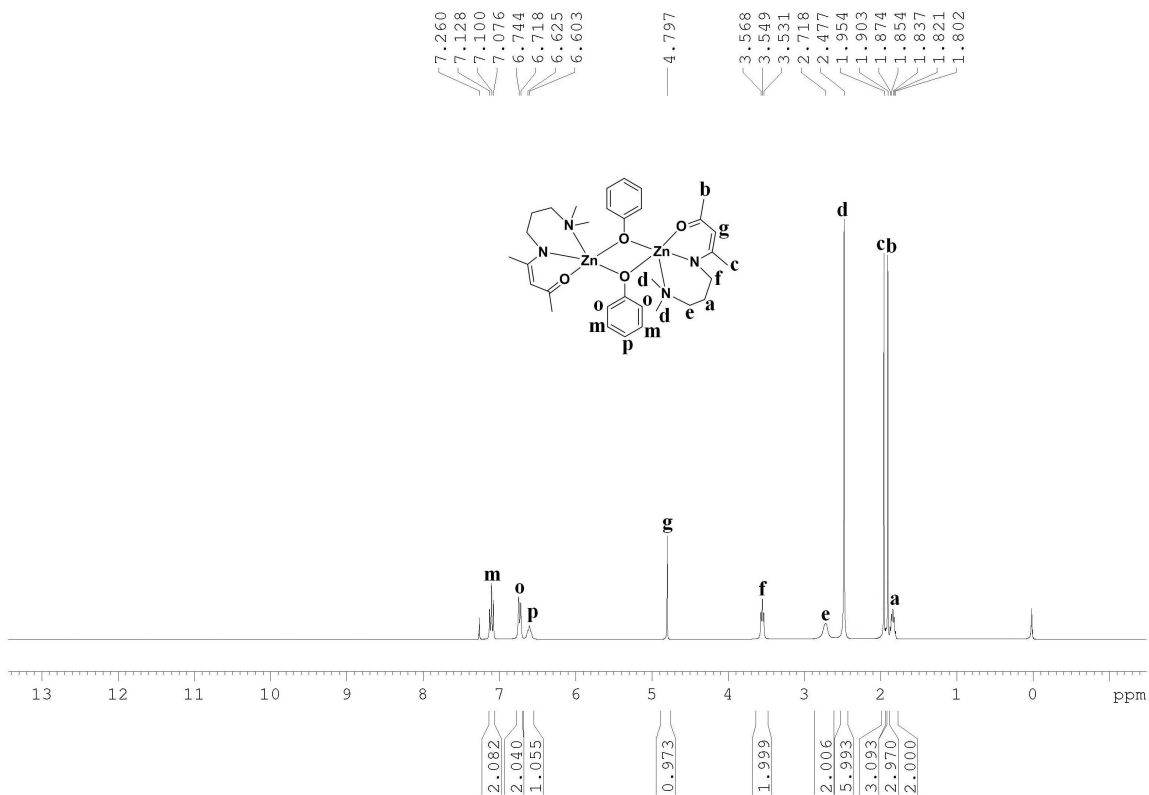


Fig. S18. ^1H NMR (300 MHz, CDCl_3 , 25 °C) spectrum of 8

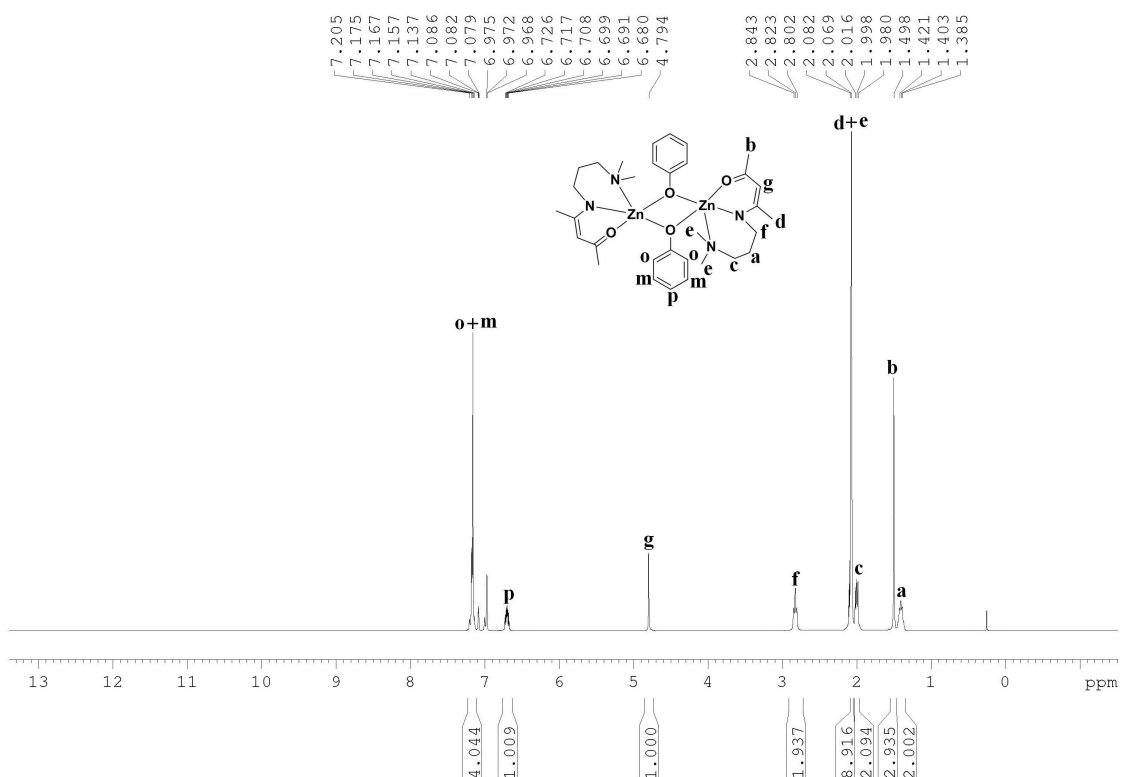


Fig. S19. ^1H NMR (300 MHz, Toluene-d8, 40 °C) spectrum of **8**

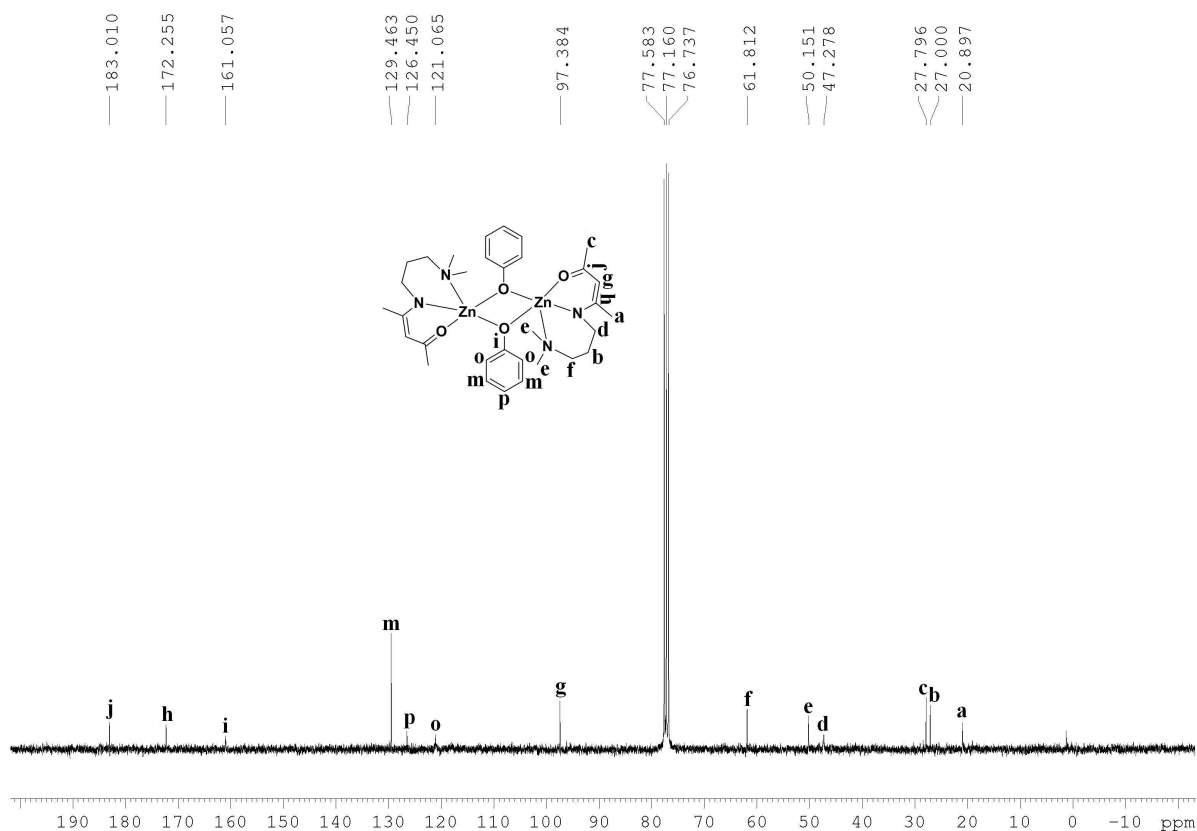


Fig. S20. ^{13}C NMR (300 MHz, CDCl_3 , 25 °C) spectrum of **8**

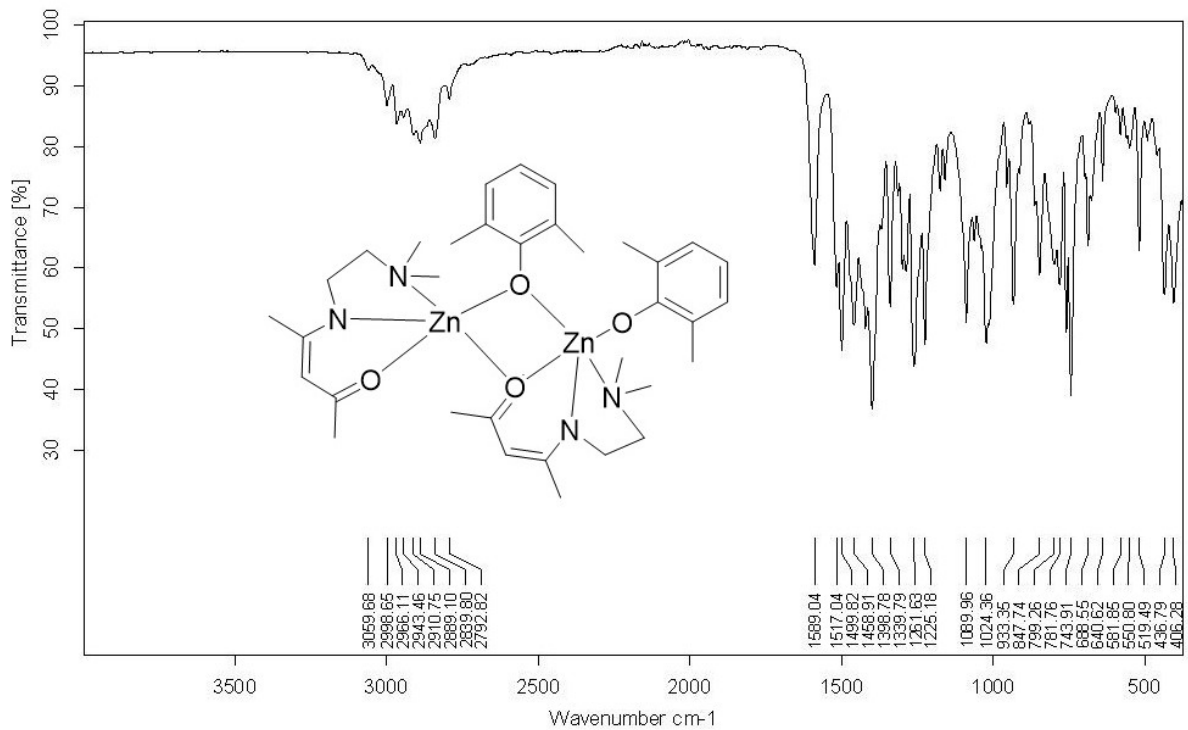


Fig. S21. AFT-IR spectrum of **1**

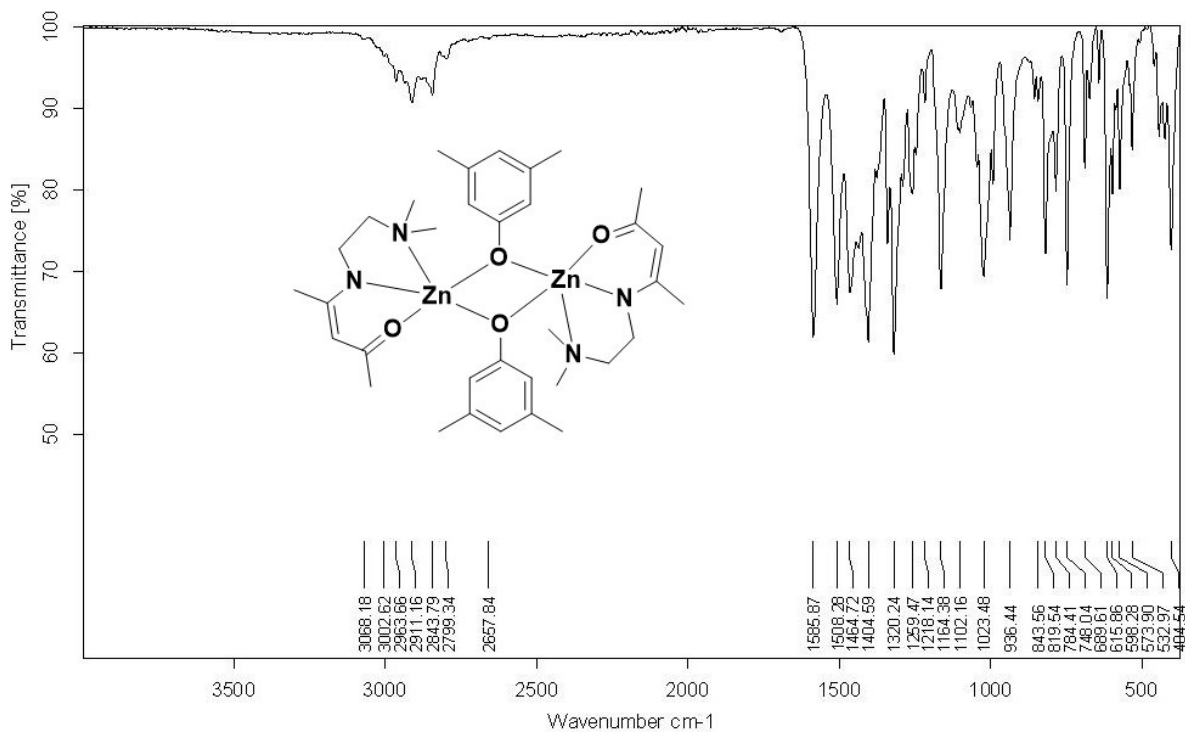


Fig. S22. AFT-IR spectrum of **2**

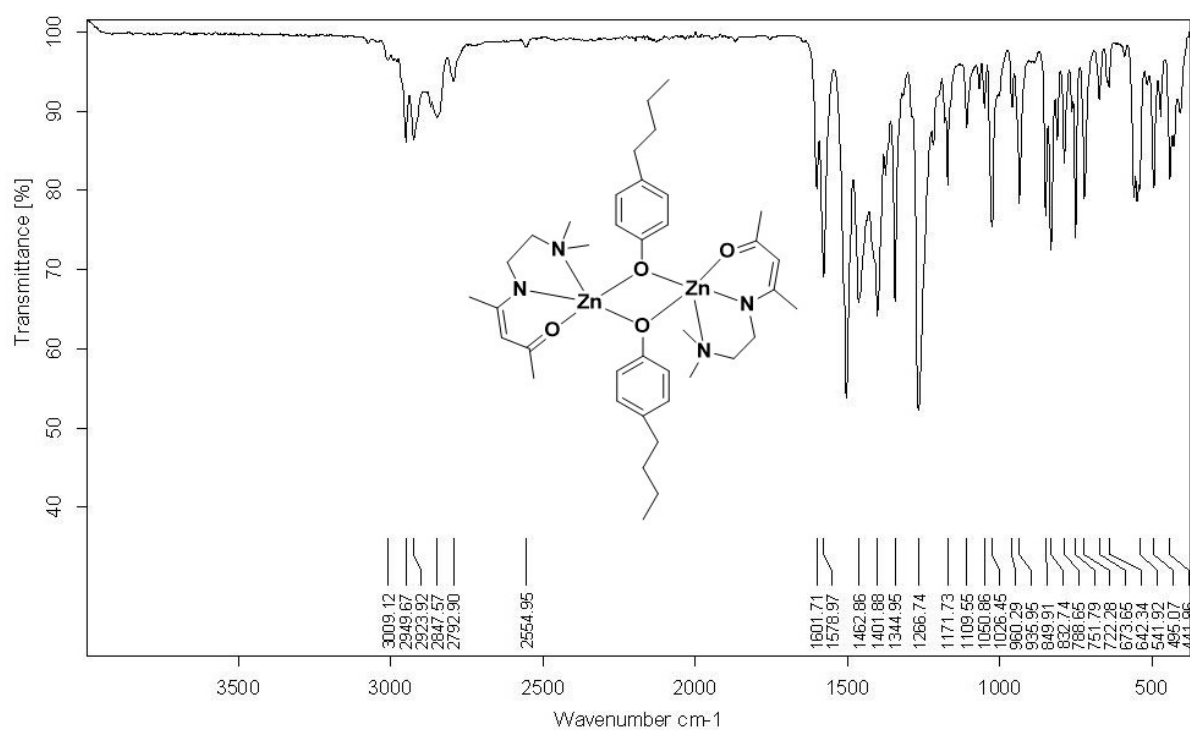


Fig. S23. AFT-IR spectrum of **3**

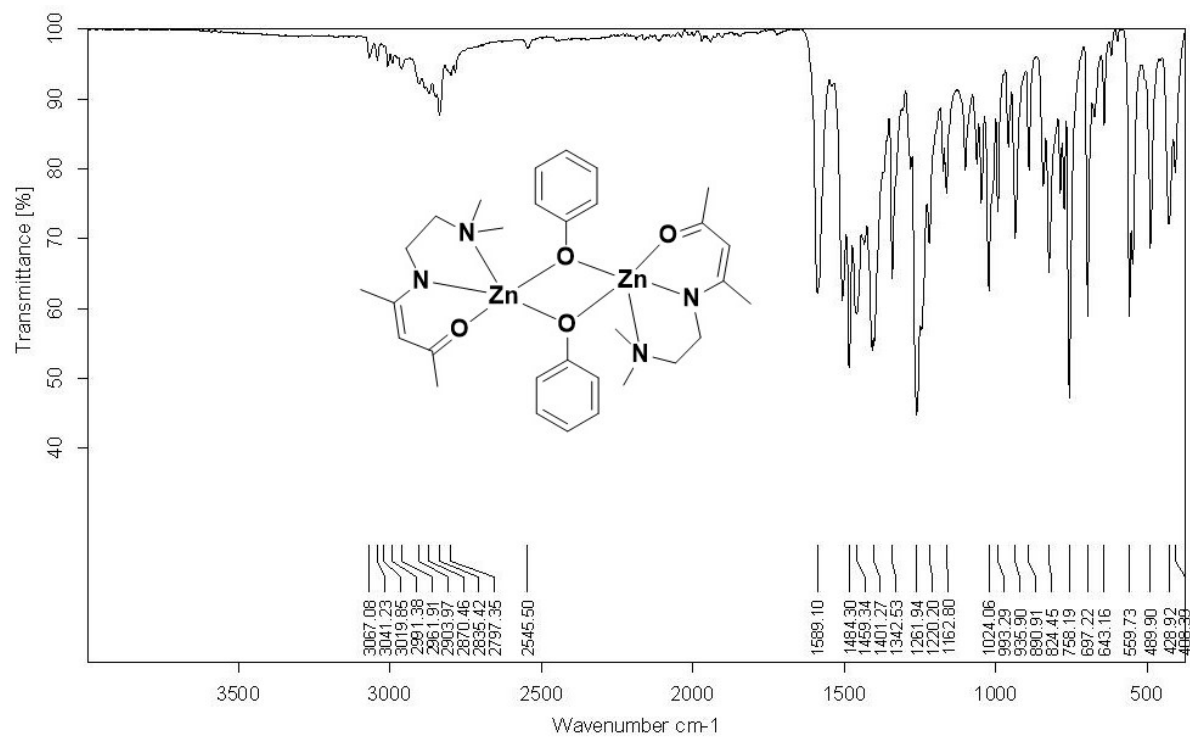


Fig. S24. AFT-IR spectrum of **4**

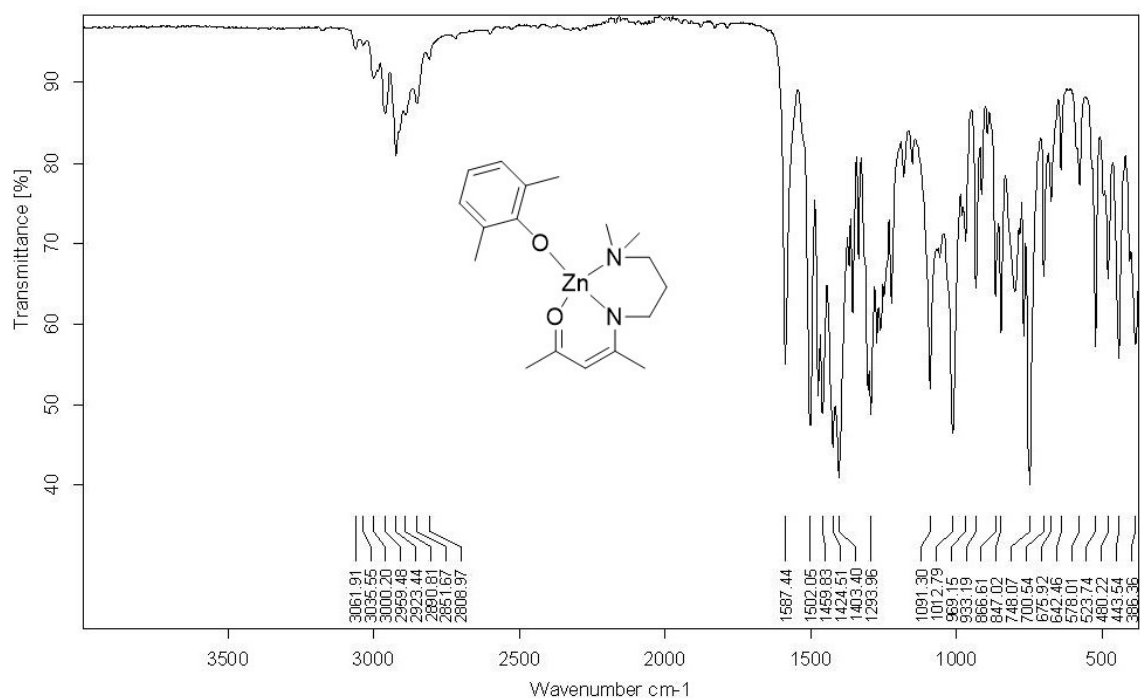


Fig. S25. AFT-IR spectrum of **5**

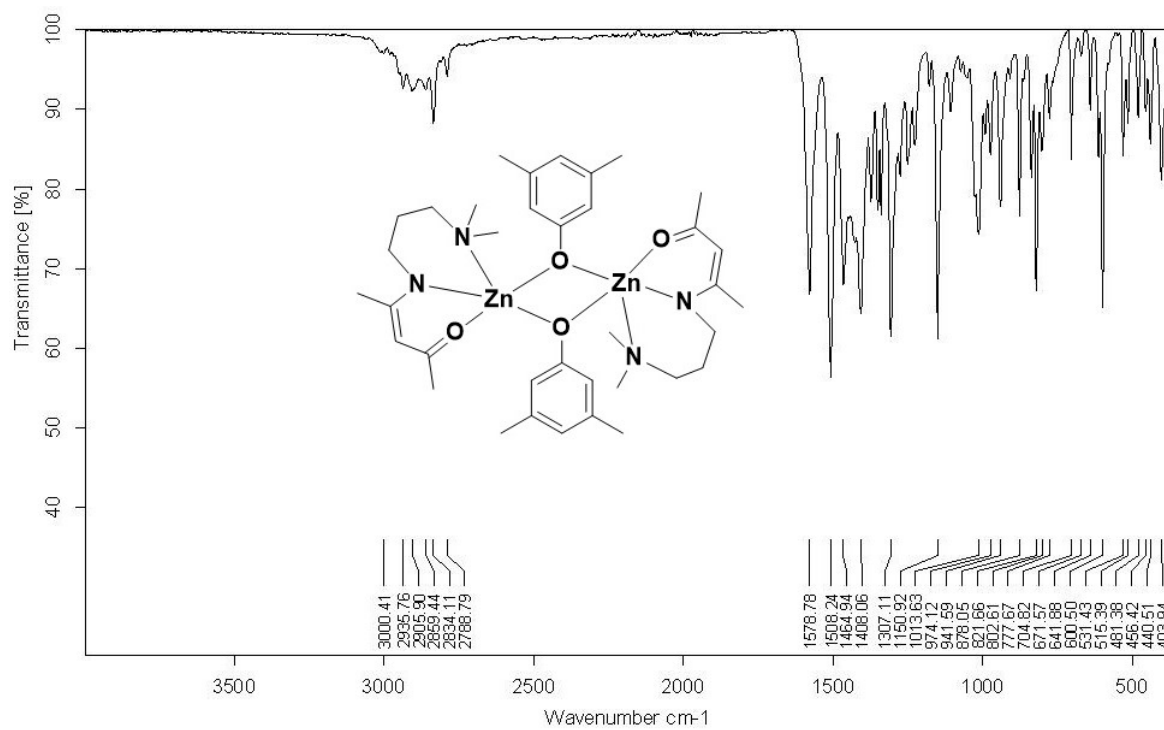


Fig. S26. AFT-IR spectrum of **6**

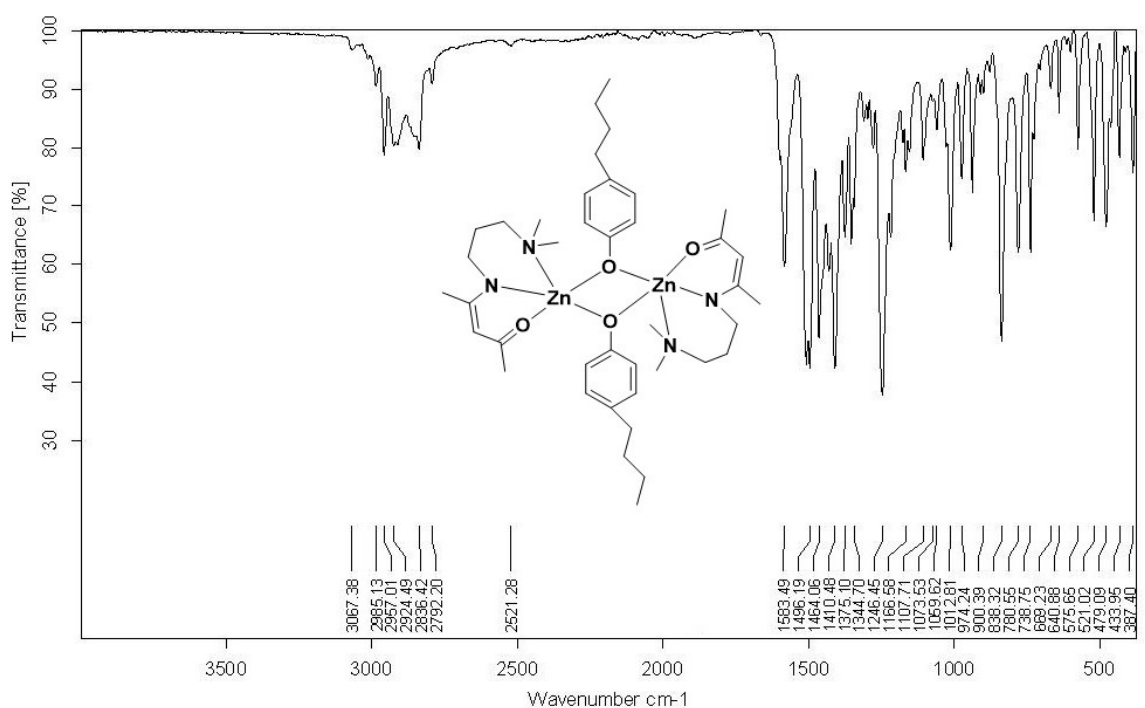
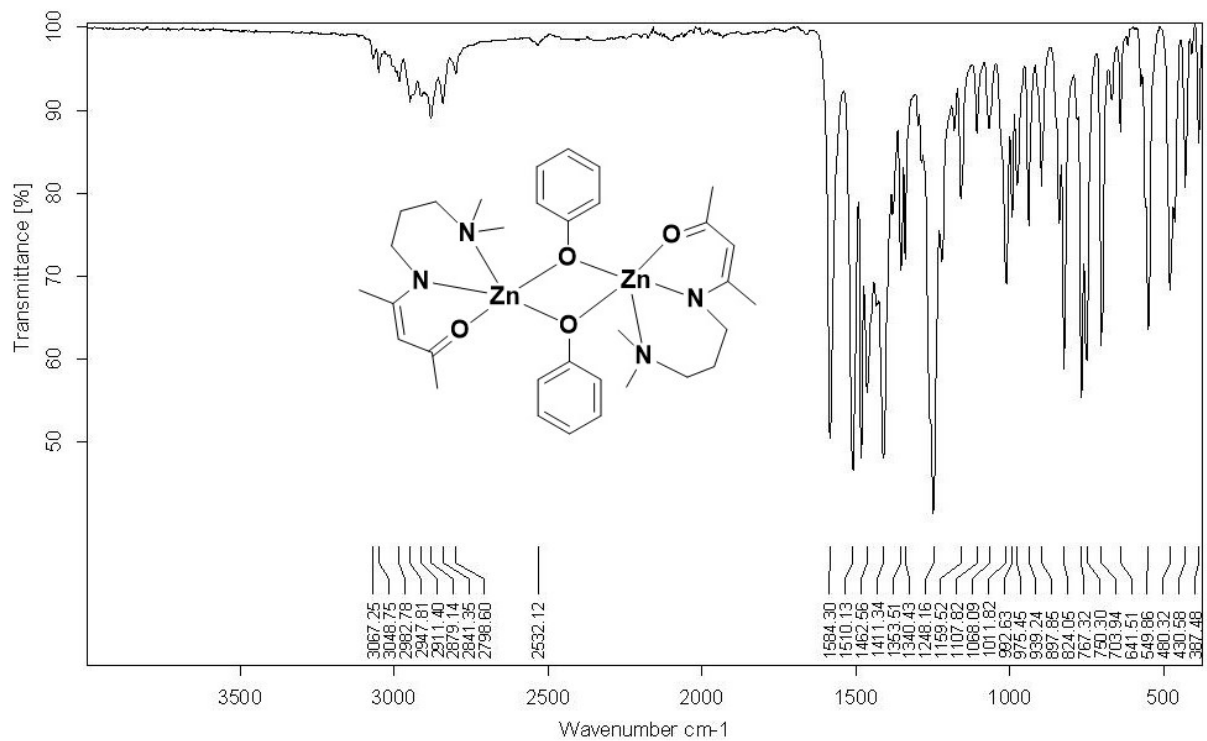


Fig. S27. AFT-IR spectrum of 7



S28. AFT-IR spectrum of 8

Fig.

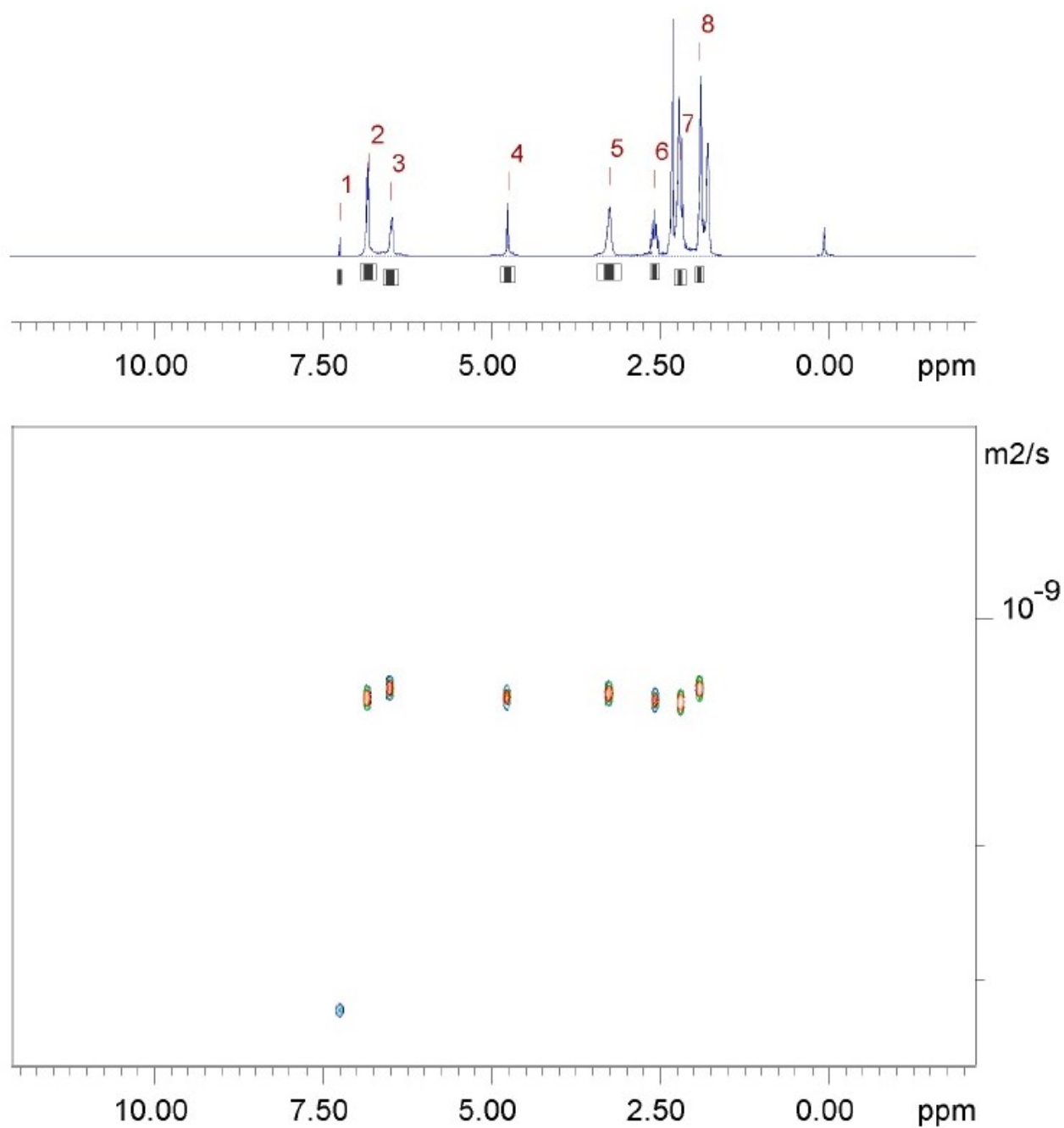


Fig S29. DOSY spectrum of (300 MHz, CDCl₃, 25 °C) spectrum of **1**

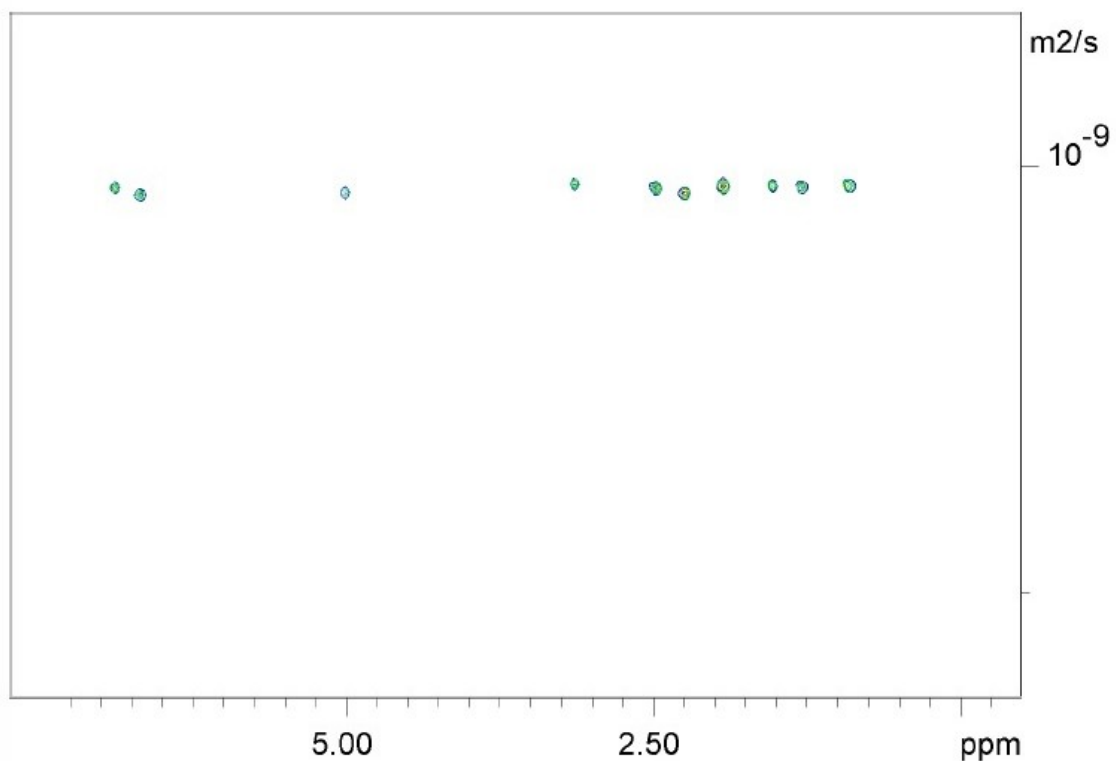
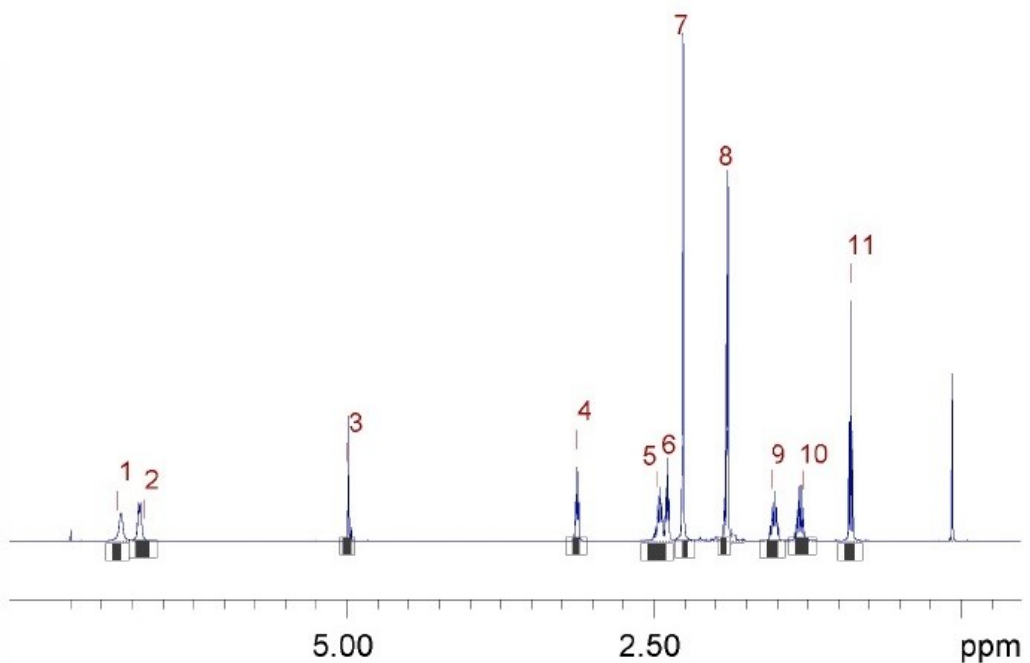


Fig S30. DOSY spectrum of (300 MHz, CDCl₃, 25 °C) spectrum of **3**

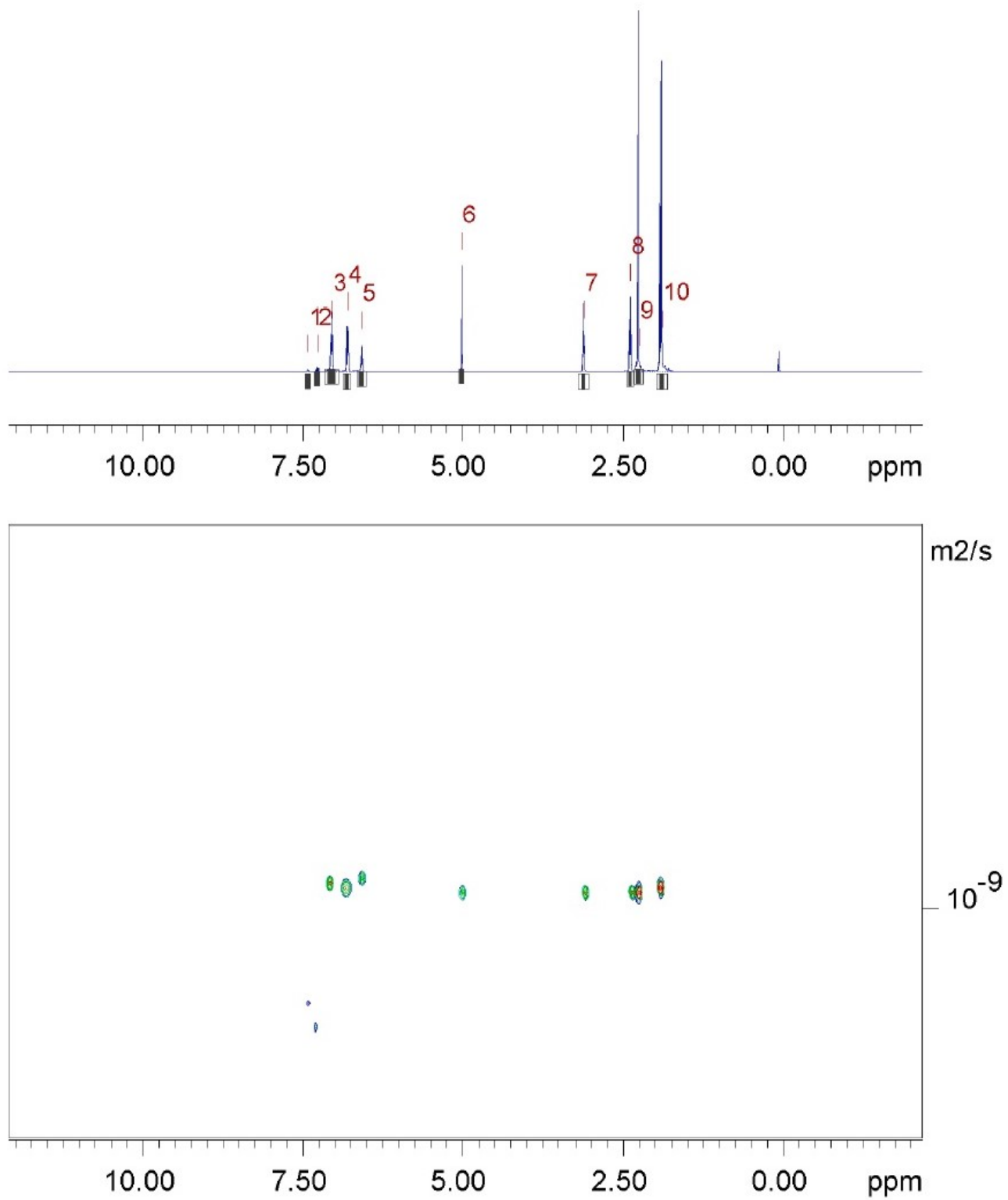


Fig S31. DOSY spectrum of (300 MHz, CDCl₃, 25 °C) spectrum of **4**

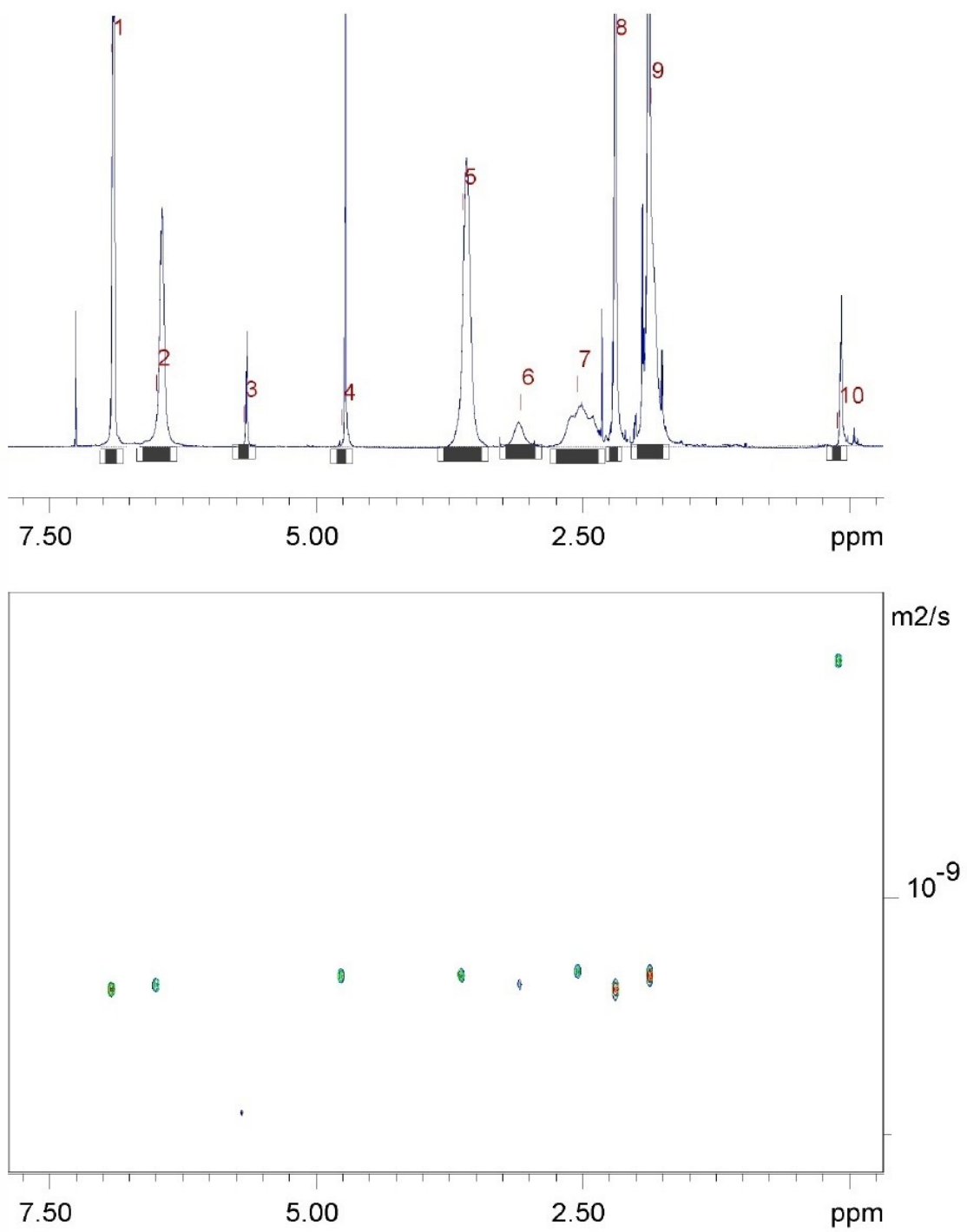


Fig S32. DOSY spectrum of (300 MHz, CDCl₃, 25 °C) spectrum of **5**

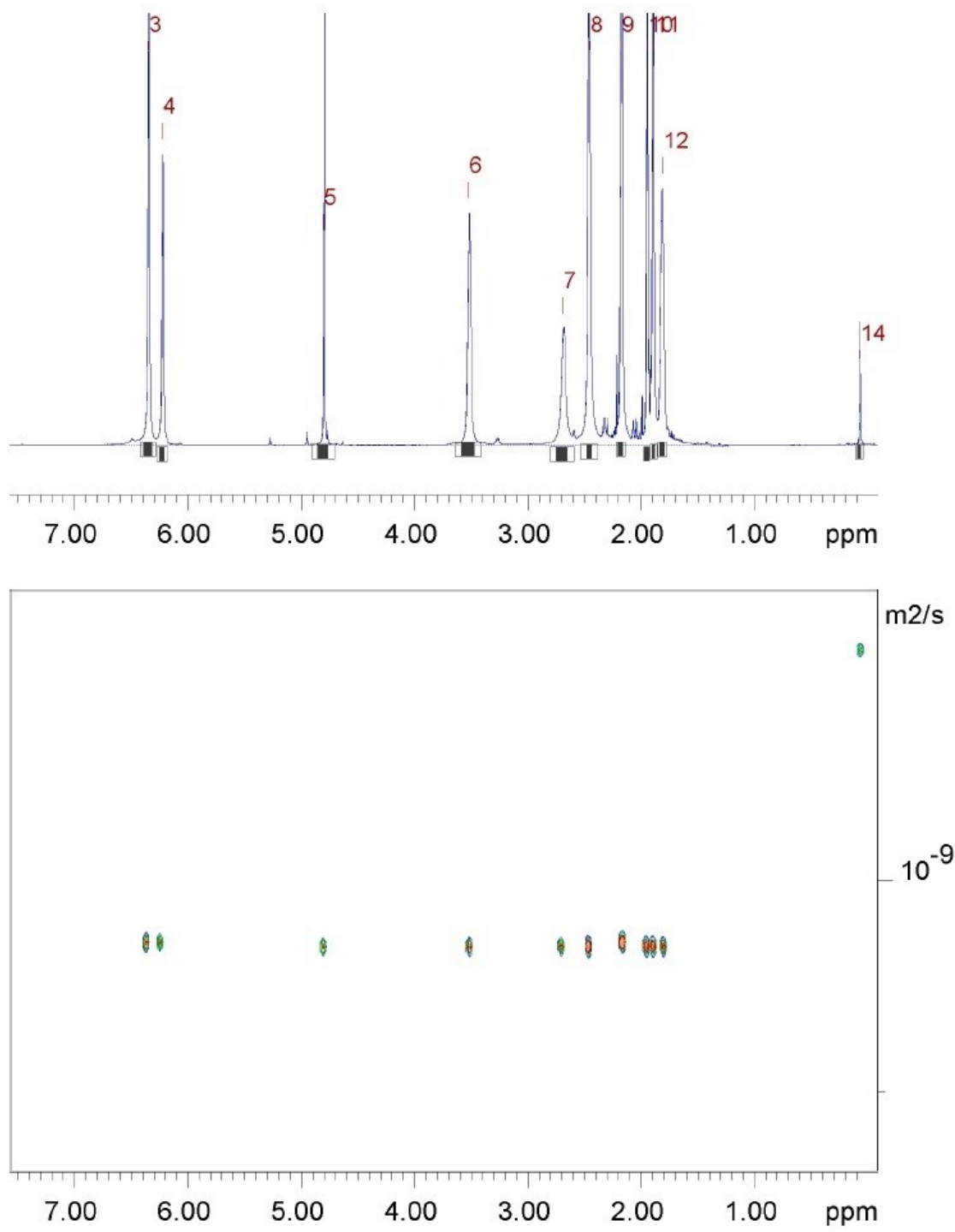


Fig S33. DOSY spectrum of (300 MHz, CDCl₃, 25 °C) spectrum of **6**

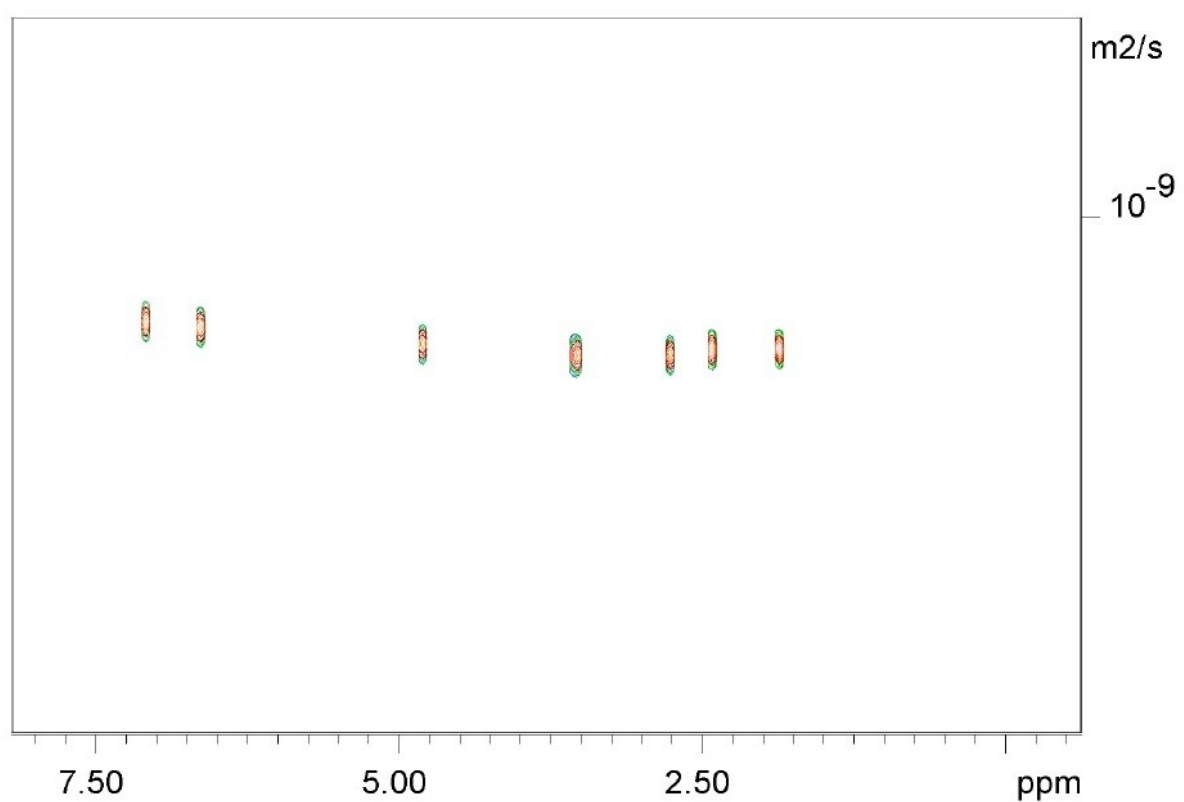
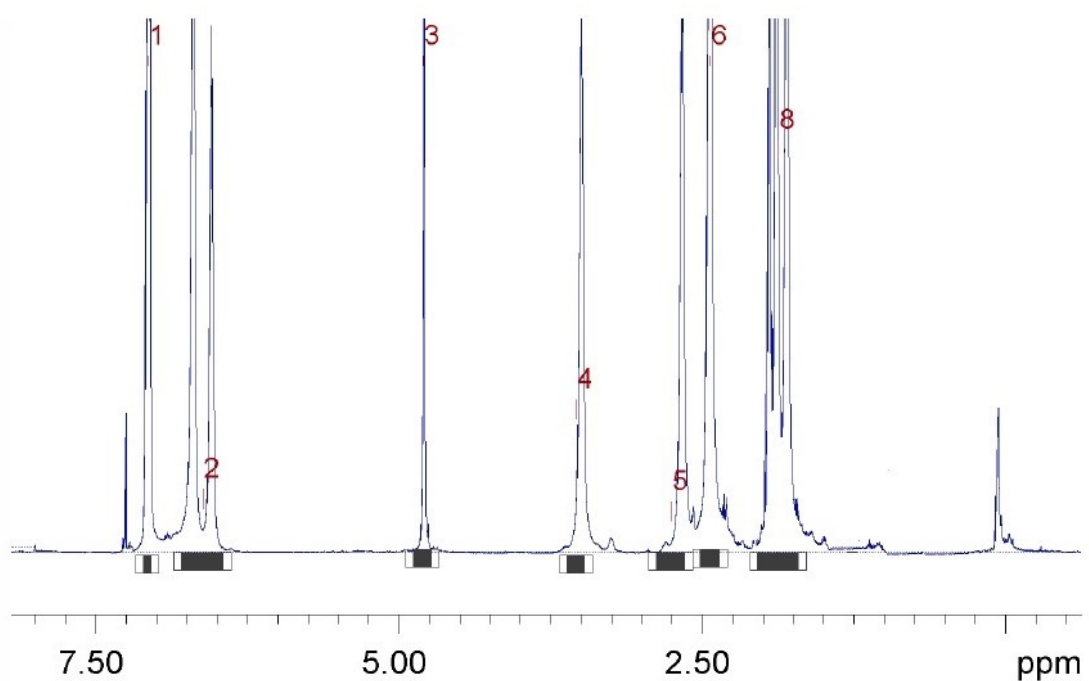


Fig S34. DOSY spectrum of (300 MHz, CDCl₃, 25 °C) spectrum of **8**

Table S1 Crystal data for compound **1**, **2**, **3** and **4**

Compounds	1	2	3	4
Empirical formula	C ₃₄ H ₅₂ N ₄ O ₄ Zn ₂	C ₃₄ H ₅₂ N ₄ O ₄ Zn ₂	C ₃₈ H ₆₀ N ₄ O ₄ Zn ₂	C ₃₀ H ₄₄ N ₄ O ₄ Zn ₂
Formula weight (Da)	711.53	711.53	767.64	655.43
T /K	100(1)	100(2)	100(2)	100(1)
Wavelength (Å)	0.71073	0.71073	0.71073	0.71073
Crystal system,	Monoclinic	Triclinic	Monoclinic	Monoclinic
Space group	P2 ₁ /c	P-1	P2 ₁ /c	P2 ₁ /c
a /Å	9.8530(6)	8.6700(9)	12.0348(9)	9.4005(4)
b /Å	17.8299(10)	10.4507(10)	10.2358(8)	17.0978(8)
c /Å	19.6519(12)	11.2159(11)	15.5503(11)	10.5776(5)
α (°)	90	67.038(4)	90	90
β (°)	92.240(2)	72.090(5)	97.039	116.049(2)
γ (°)	90	81.040(5)	90	90
V (Å ³)	3449.8(4)	889.64(16)	1901.1(2)	1527.41(12)
Z, Calculated density (g cm ⁻³)	4, 1.370	1, 1.328	2, 1.341	2, 1.425
Absorption coefficient (mm ⁻¹)	1.432	1.388	1.341	1.611
Crystal size (mm)	0.230 x 0.180 x 0.050	0.458 x 0.194 x 0.100	0.189 x 0.128 x 0.078	0.250 x 0.180 x 0.130
Theta range for data collection (°)	2.068 to 30.645	2.049 to 33.39	1.705 to 33.167	2.412 to 30.525
Reflections collected/unique	82400	54063	61470	28881
Independent reflections	10544	6580	7035	4582
Data/restraints/parameters	8403 / 0 / 438	6580 / 258 / 280	7035 / 0 / 222	4254 / 0 / 185
Goodness-of-fit on F ²	1.089	1.051	1.062	1.093
Final R indices [I > 2σ(I)]	R1 = 0.0379 wR2 = 0.0850	R1 = 0.0239 wR2 = 0.0607	R1 = 0.0293 wR2 = 0.0646	R1 = 0.0216 wR2 = 0.0589
R indices (all data)	R1 = 0.0565 wR2 = 0.0947	R1 = 0.0285 wR2 = 0.0634	R1 = 0.0520 wR2 = 0.0736	R1 = 0.0244 wR2 = 0.0604

Table S2 Crystal data for compound **5**, **6**, **7** and **8**

Compounds	5	6	7	8·C₇H₈
Empirical formula	C ₁₈ H ₂₈ N ₂ O ₂ Zn	C ₃₆ H ₅₆ N ₄ O ₄ Zn ₂	C ₄₀ H ₆₄ N ₄ O ₄ Zn ₂	C ₃₂ H ₄₈ N ₄ O ₄ Zn ₂ ,C ₇ H ₈
Formula weight (Da)	369.79	739.58	795.69	775.61
T/K	100(1)	100(2)	105(2)	100(1)
Wavelength (Å)	0.71073	0.71073	0.71073	0.71073
Crystal system,	Monoclinic	Tetragonal	Monoclinic	Monoclinic
Space group	<i>P</i> 2 ₁	<i>I</i> 4 ₁ / <i>a</i>	<i>P</i> 2 ₁ / <i>c</i>	<i>P</i> 2 ₁
<i>a</i> /Å	8.323(2)	25.6258(16)	9.9064(12)	10.6474(5)
<i>b</i> /Å	12.343(3)	25.6258(16)	14.1071(16)	15.1340(6)
<i>c</i> /Å	8.800(2)	11.1739(7)	14.2769(15)	12.4806(6)
α (°)	90	90	90	90
β (°)	91.073(6)	90	94.676(5)	103.622(2)
γ (°)	90	90	90	90
V (Å ³)	903.9(4)	7337.7	1988.6(4)	1954.52(15)
Z, Calculated density (g cm ⁻³)	2, 1.359	8, 1.339	2, 1.329	2, 1.318
Absorption coefficient (mm ⁻¹)	1.369	1.349	1.250	1.270
Crystal size (mm)	0.440 x 0.360 x 0.280	0.371 x 0.200 x 0.160	0.265 x 0.230 x 0.094	0.430 x 0.320 x 0.180
Theta range for data collection (°)	2.843° to 30.586	1.589 to 33.223	2.033 to 46.702	2.152° to 30.689°
Reflections collected/unique	15057	87544	109018	48987
Independent reflections	5318	7011	13517	11048
Data/restraints/parameters	5154 / 1 / 215	7011 / 0 / 214	13517 / 0 / 231	10383 / 1 / 451
Goodness-of-fit on <i>F</i> ²	1.051	1.050	1.027	1.050
<i>x</i> (Flack)	0.022(3)	—	—	0.023(3)
Final <i>R</i> indices [<i>I</i> > 2σ(<i>I</i>)]	<i>R</i> 1 = 0.0182 <i>wR</i> 2 = 0.0479	<i>R</i> 1 = 0.0238 <i>wR</i> 2 = 0.0616	<i>R</i> 1 = 0.0278 <i>wR</i> 2 = 0.0718	<i>R</i> 1 = 0.0202 <i>wR</i> 2 = 0.0513
<i>R</i> indices (all data)	<i>R</i> 1 = 0.0191 <i>wR</i> 2 = 0.0482	<i>R</i> 1 = 0.0290 <i>wR</i> 2 = 0.0650	<i>R</i> 1 = 0.0468 <i>wR</i> 2 = 0.0796	<i>R</i> 1 = 0.0229 <i>wR</i> 2 = 0.0522

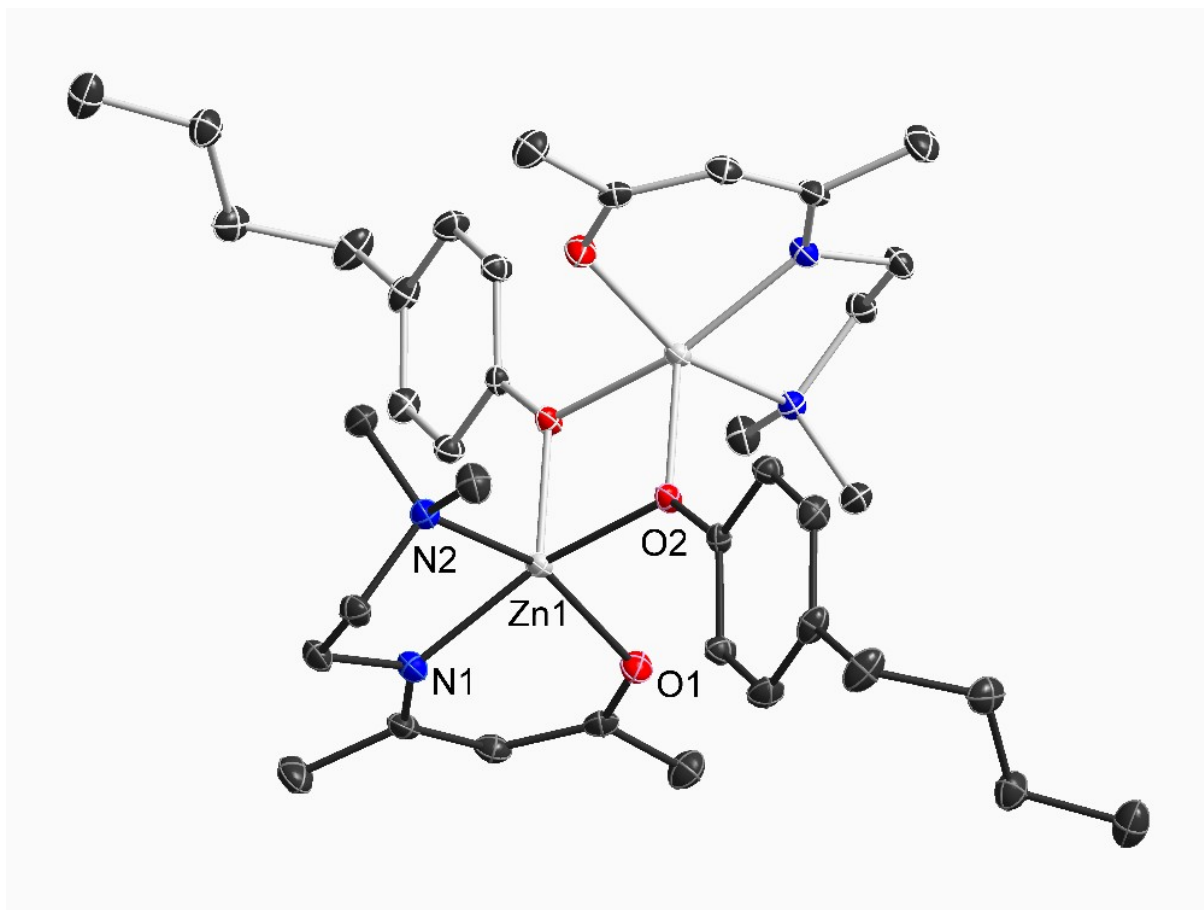


Fig. S35. ORTEP representation of solid-state structure of compound **3**. H atoms have been omitted for clarity and thermal ellipsoids are shown with 50% probability level. i $1-x$, $2-y$, $1-z$. Selected bond lengths [\AA] and angles [$^\circ$]: Zn(1)-O(2)^{*i*} 2.0044(9), Zn(1)-N(1) 2.0348(11), Zn(1)-O(2) 2.0370(9), Zn(1)-O(1) 2.0499(9), Zn(1)-N(2) 2.2473(11), O(2)^{*i*}-Zn(1)-N(1) 119.87(4), O(2)^{*i*}-Zn(1)-O(2) 80.03(4), N(1)-Zn(1)-O(2) 159.14(4), O(2)^{*i*}-Zn(1)-O(1) 104.99(4), N(1)-Zn(1)-O(1) 88.18(4), O(2)-Zn(1)-O(1) 92.63(4), O(2)^{*i*}-Zn(1)-N(2) 97.76(4), N(1)-Zn(1)-N(2) 80.26(4), O(2)-Zn(1)-N(2) 91.44(4), O(1)-Zn(1)-N(2) 157.25(4).

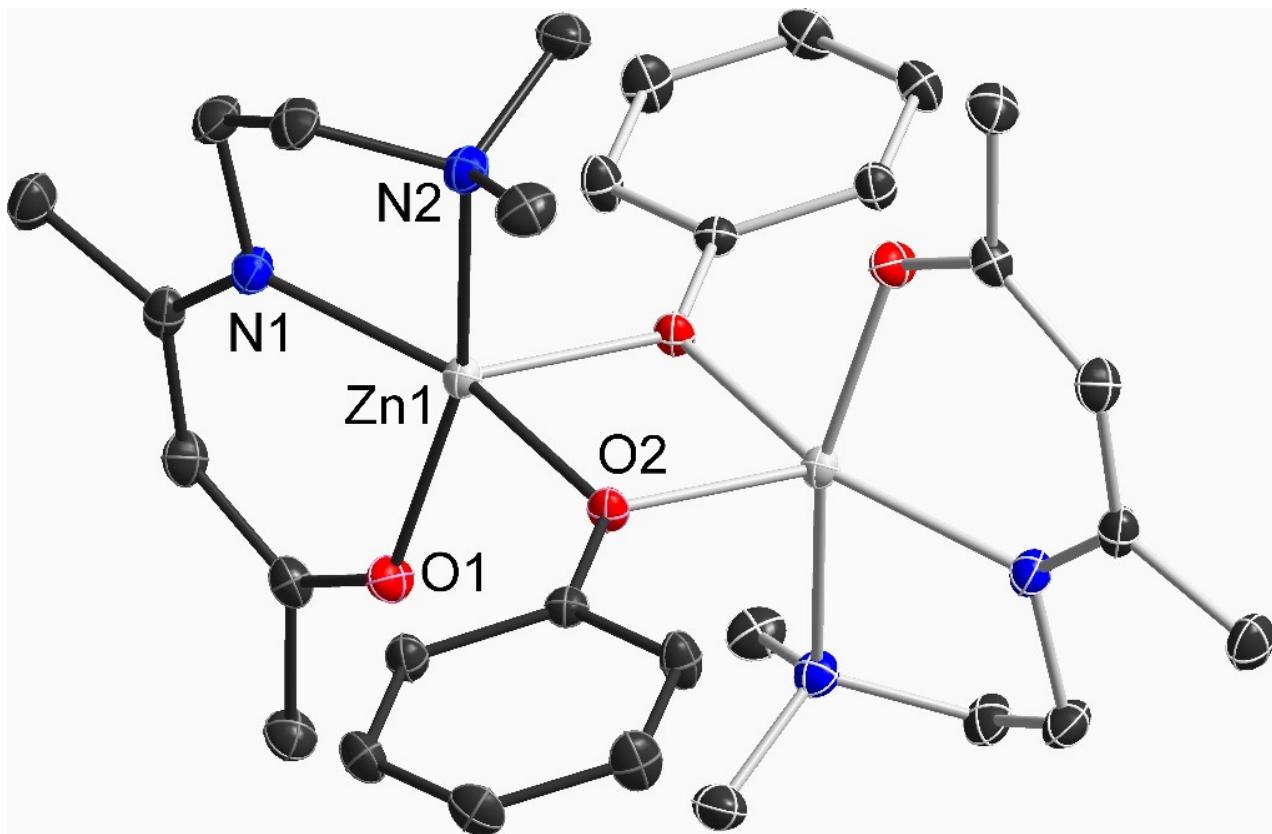


Fig. S36. ORTEP representation of solid-state structure of compound **4**. H atoms have been omitted for clarity and thermal ellipsoids are shown with 50% probability level. $i -x, 1-y, -z$. Selected bond lengths [\AA] and angles [$^\circ$]: Zn(1)-O(2) i 2.0077(8), Zn(1)-N(1) 2.0296(10), Zn(1)-O(1) 2.0339(8), Zn(1)-O(2) 2.0395(8), Zn(1)-N(2) 2.2433(10), O(2) i -Zn(1)-N(1) 124.33(4), O(2) i -Zn(1)-O(1) 101.30(3), N(1)-Zn(1)-O(1) 88.73(4), O(2) i -Zn(1)-O(2) 80.48(3), N(1)-Zn(1)-O(2) 154.78(4), O(1)-Zn(1)-O(2) 90.62(3), O(2) i -Zn(1)-N(2) 97.84(3), N(1)-Zn(1)-N(2) 81.35(4), O(1)-Zn(1)-N(2) 160.82(4), O(2)-Zn(1)-N(2) 91.45(3).

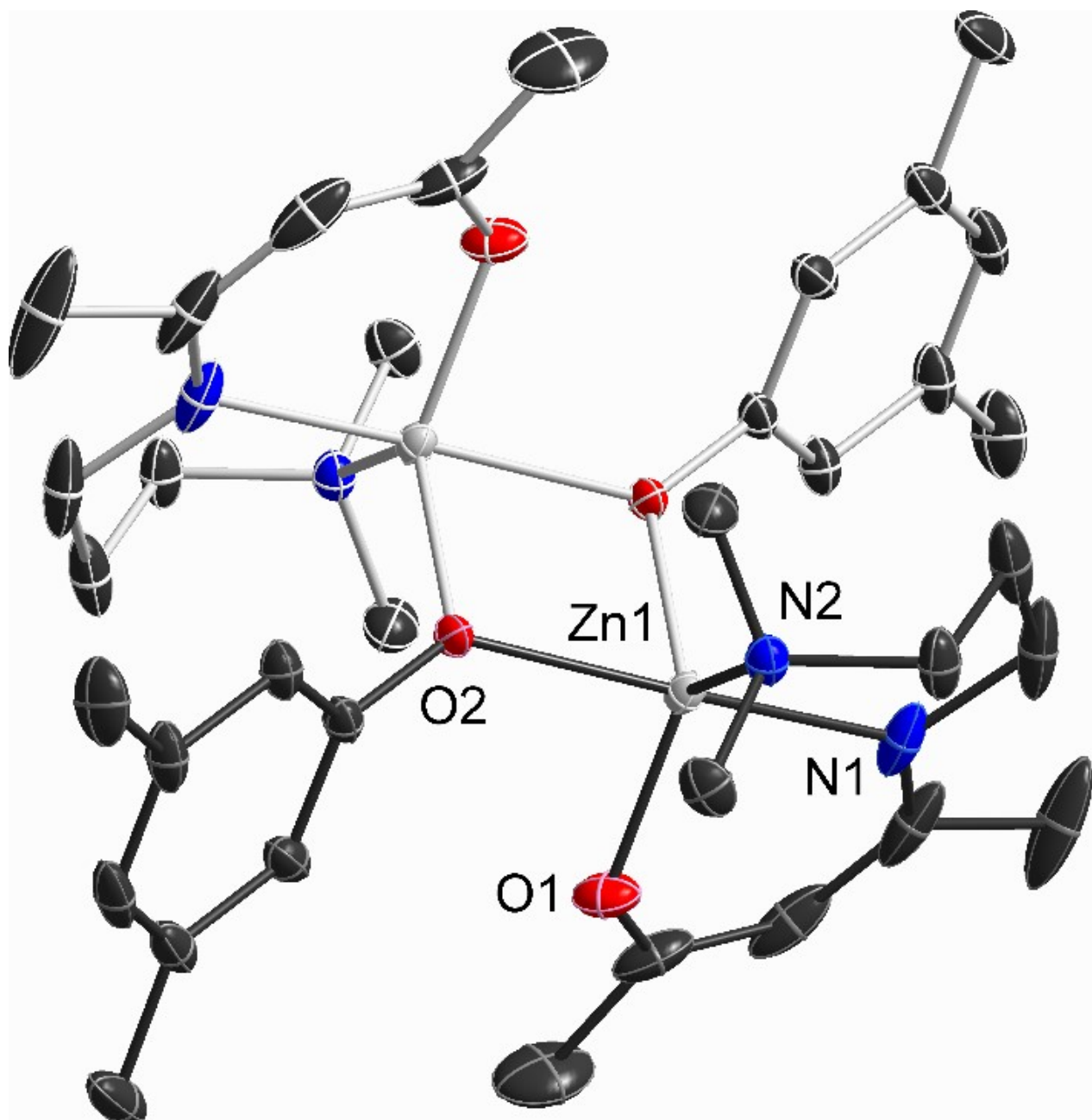


Fig. S37. ORTEP representation of solid-state structure of compound **6**. H atoms have been omitted for clarity and thermal ellipsoids are shown with 50% probability level. i $2-x$, $1-y$, $-z$. Selected bond lengths [Å] and angles [°]: Zn(1)-O(1) 1.9589(8), Zn(1)-O(2)ⁱ 2.0034(7), Zn(1)-N(1) 2.0696(8) Zn(1)-N(2) 2.1349(8), Zn(1)-O(2) 2.1420(6), O(1)-Zn(1)-O(2)ⁱ 120.94(3), O(1)-Zn(1)-N(1) 91.17(4), O(2)ⁱ-Zn(1)-N(1) 95.59(3), O(1)-Zn(1)-N(2) 121.32(3), O(2)ⁱ-Zn(1)-N(2) 116.39(3), N(1)-Zn(1)-N(2) 94.92(3), O(1)-Zn(1)-O(2) 88.29(3), O(2)ⁱ-Zn(1)-O(2) 79.53(3), N(1)-Zn(1)-O(2) 173.91(3), N(2)-Zn(1)-O(2) 90.54(3), C(3)-O(1)-Zn(1) 121.13(8).

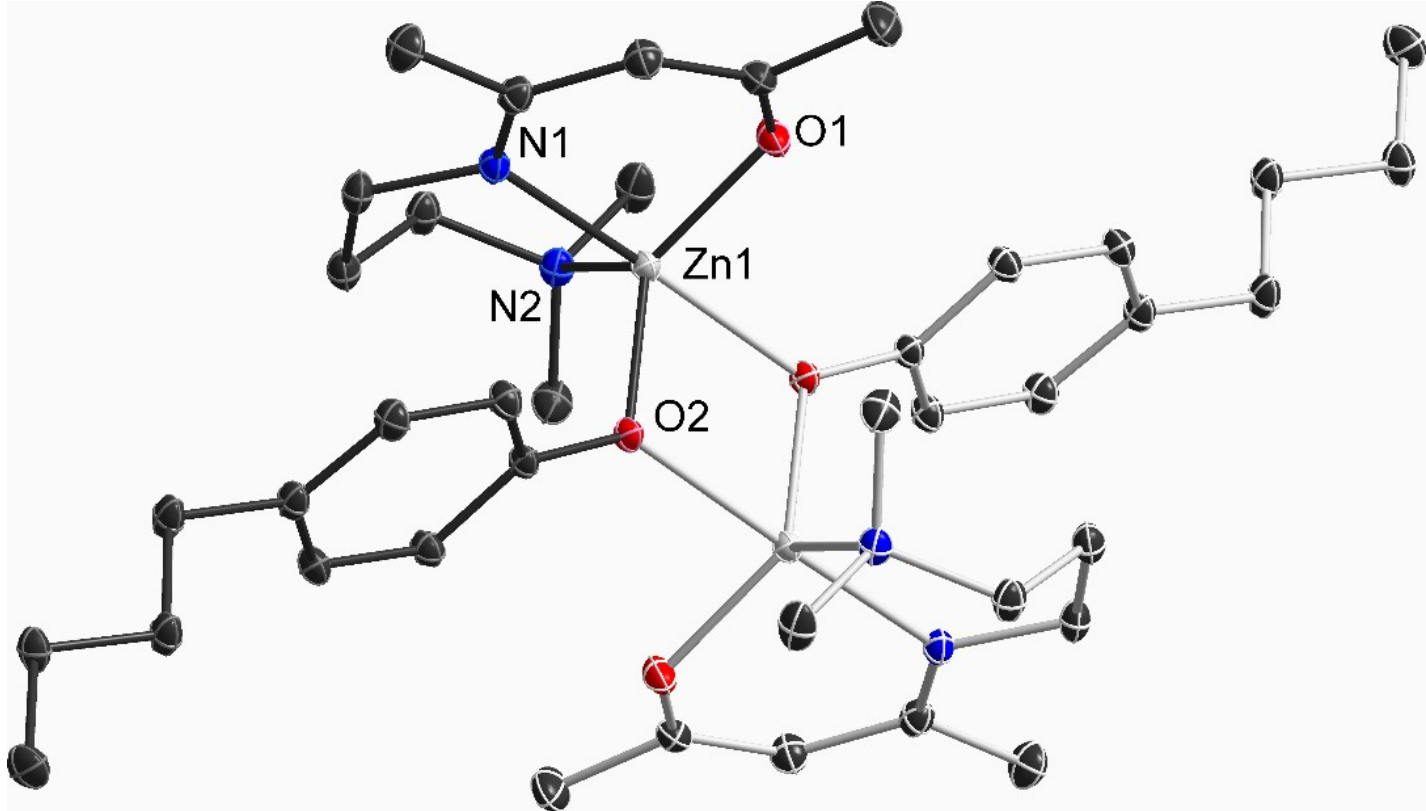


Fig. S38. ORTEP representation of solid-state structure of compound 7. H atoms have been omitted for clarity and thermal ellipsoids are shown with 50% probability level. i $1-x$, $-y$, $1-z$. Selected bond lengths [Å] and angles [°]: Zn(1)-O(1) 1.9681(6), Zn(1)-O(2) 2.0022(5), Zn(1)-N(1) 2.0897(6), Zn(1)-N(2) 2.1293(6), Zn(1)-O(2)ⁱ 2.1598(5), O(1)-Zn(1)-O(2) 119.28(2), O(1)-Zn(1)-N(1) 91.57(2), O(2)-Zn(1)-N(1) 98.50(2), O(1)-Zn(1)-N(2) 125.35(2), O(2)-Zn(1)-N(2) 113.36(2), N(1)-Zn(1)-N(2) 94.43(2), O(1)-Zn(1)-O(2)ⁱ 88.39(2), O(2)-Zn(1)-O(2)ⁱ 77.80(2), N(1)-Zn(1)-O(2)ⁱ 175.70(2), N(2)-Zn(1)-O(2)ⁱ 89.09(2).

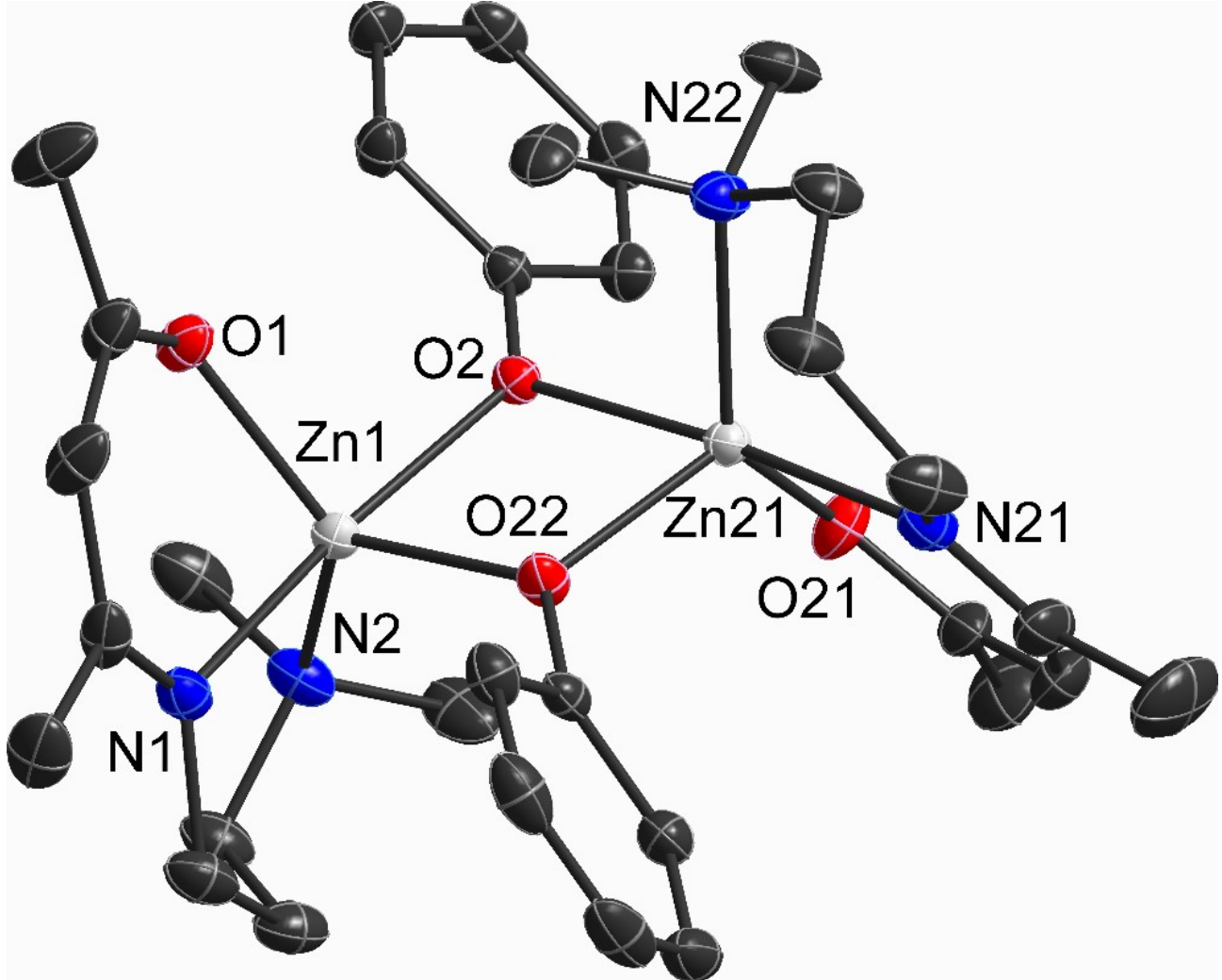


Fig. S39. ORTEP representation of solid-state structure of compound **8**. H atoms and solvent molecule have been omitted for clarity and thermal ellipsoids are shown with 50% probability level. Selected bond lengths [Å] and angles [°]: Zn(1)-O(1) 1.9789(12), Zn(1)-O(22) 2.0268(13), Zn(1)-N(1) 2.0902(14), Zn(1)-O(2) 2.1012(13), Zn(1)-N(2) 2.1174(14), Zn(21)-O(21) 1.9645(12), Zn(21)-O(22) 1.9999(13), Zn(21)-N(21) 2.0887(15), Zn(21)-O(2) 2.1385(13), Zn(21)-N(22) 2.1428(14), O(22)-Zn(21)-N(21) 98.91(6), O(21)-Zn(21)-O(2) 87.90(5), O(22)-Zn(21)-O(2) 77.76(4), N(21)-Zn(21)-O(2) 175.28(5), O(21)-Zn(21)-N(22) 130.41(6), O(22)-Zn(21)-N(22) 108.20(5), N(21)-Zn(21)-N(22) 94.25(6), O(2)-Zn(21)-N(22) 90.00(5).

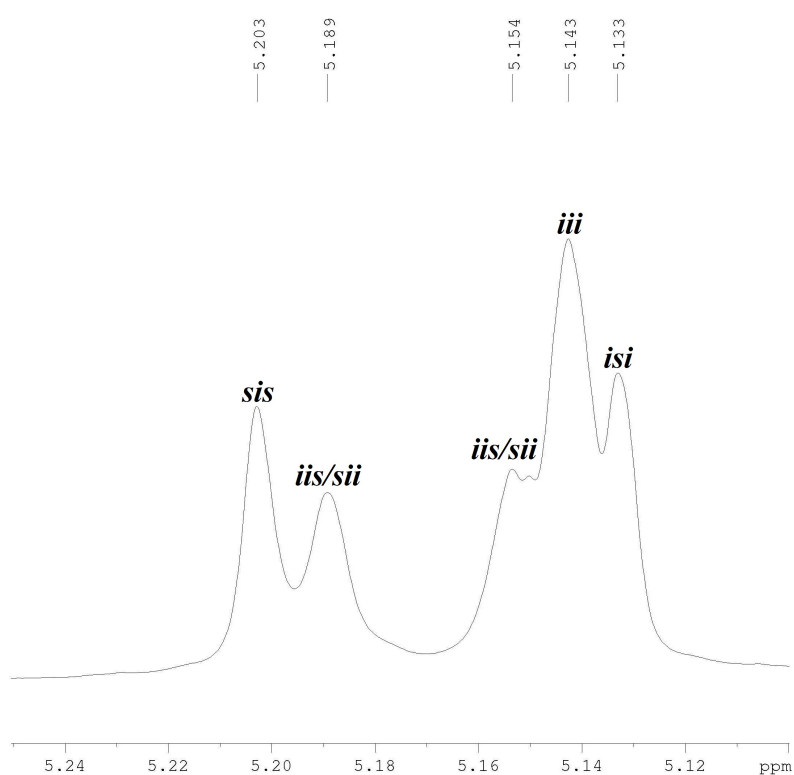


Fig S40. Homonuclear decoupled ^1H -NMR spectrum of *rac*-PLA in CDCl_3 (methine H-atom region) obtained by reaction of *rac*-LA and **1** in ratio 200:1 at 25 °C.

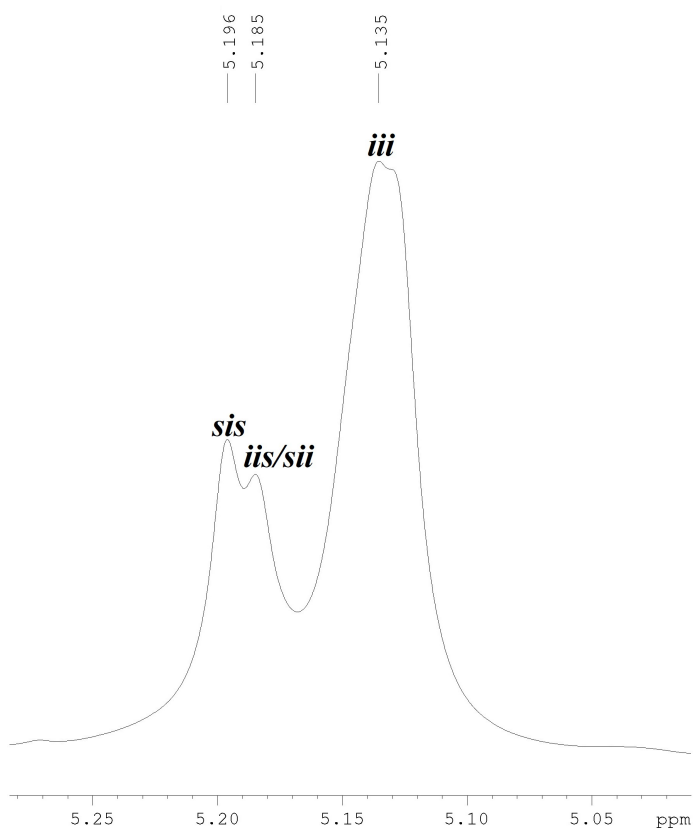


Fig S41. Homonuclear decoupled ^1H -NMR spectrum of *rac*-PLA in CDCl_3 (methine H-atom region) obtained by reaction of *rac*-LA and **5** in ratio 200:1 at 25 °C.

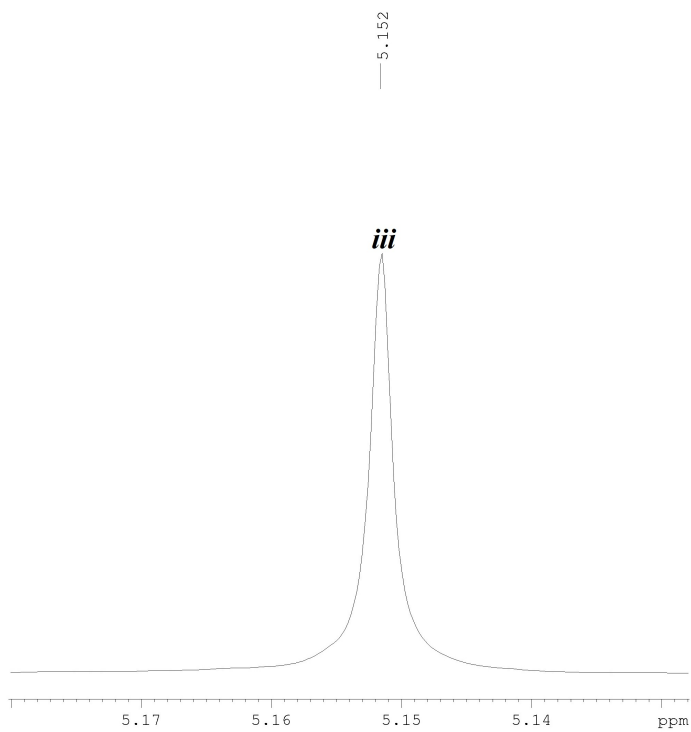


Fig S42. Homonuclear decoupled ^1H -NMR spectrum of *L*-PLA in CDCl_3 (methine H-atom region) obtained by reaction of *L*-LA and **1** in ratio 200:1 at 25 °C.

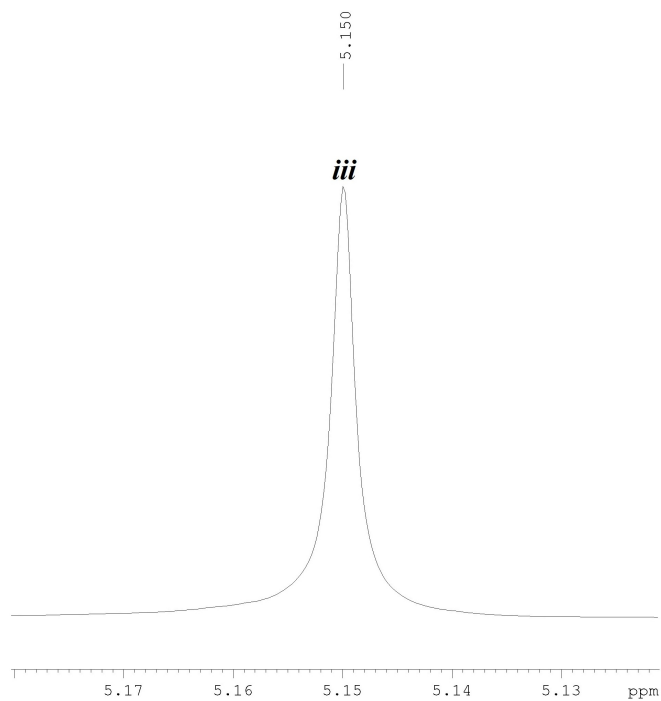


Fig S43. Homonuclear decoupled ^1H -NMR spectrum of *L*-PLA in CDCl_3 (methine H-atom region) obtained by reaction of *L*-LA and **5** in ratio 200:1 at 25 °C.

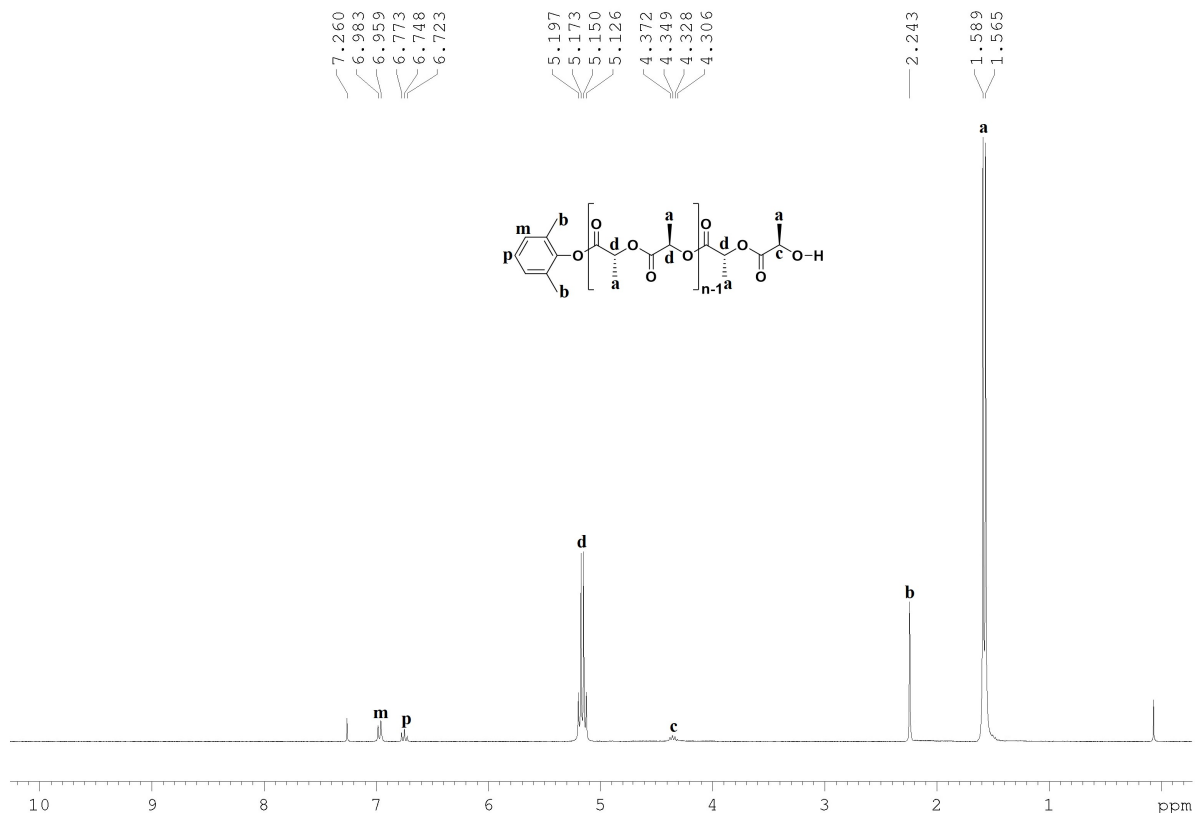


Fig S44. ^1H -NMR spectrum of *L*-PLA in CDCl_3 obtained by reaction of *L*-LA and **1** in ratio 50:1 at 25 °C in CH_2Cl_2 .

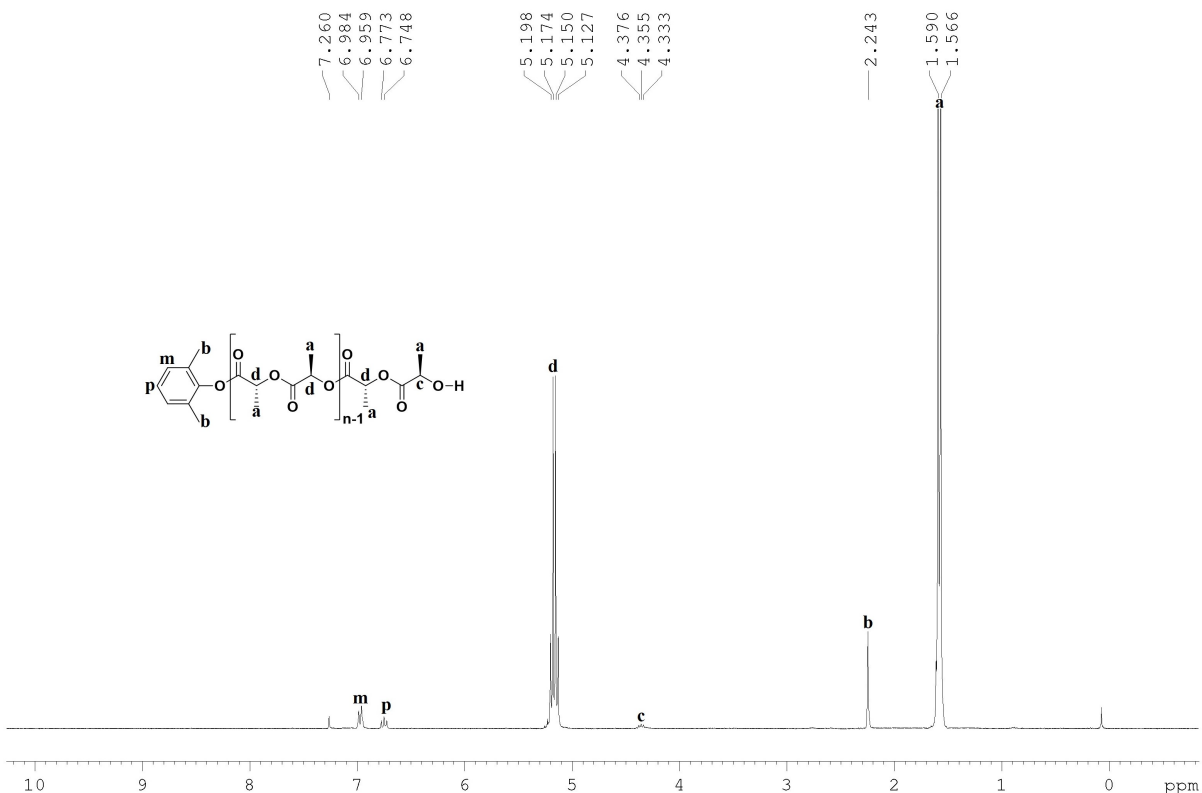


Fig S45. ^1H -NMR spectrum of *L*-PLA in CDCl_3 obtained by reaction of *L*-LA and **5** in ratio 50:1 at 25 °C in CH_2Cl_2 .

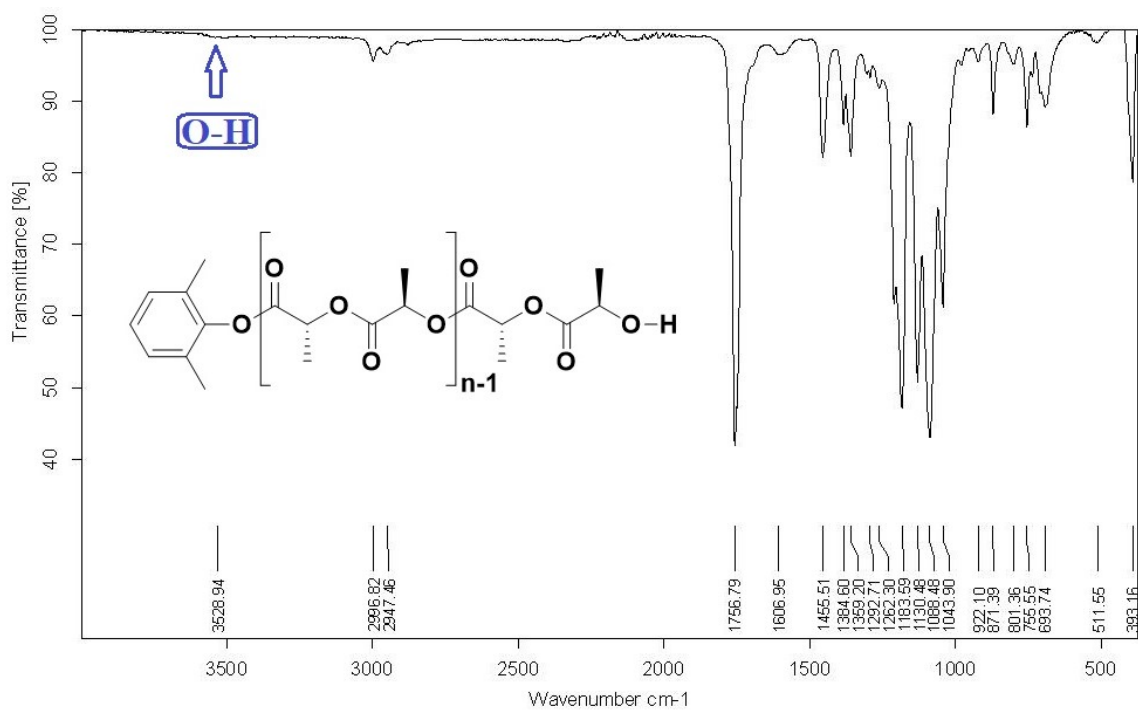


Fig S46. IR spectrum of *L*-PLA obtained by reaction of *L*-LA and **5** in ratio 50:1 at 25 °C in CH_2Cl_2 .

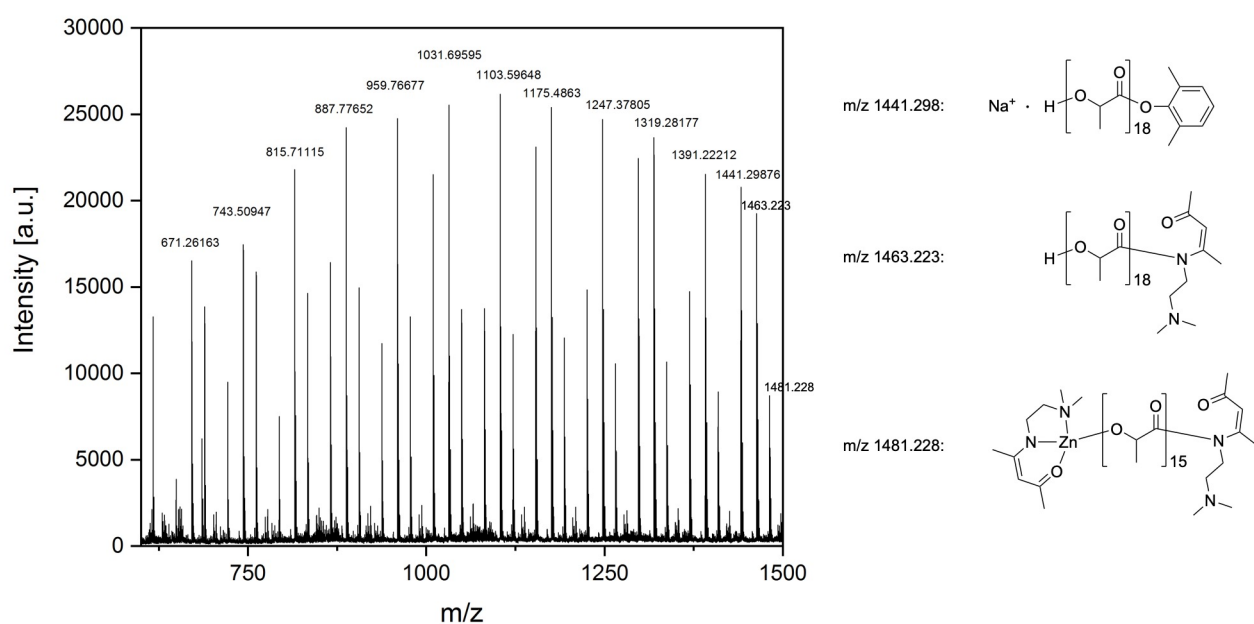


Fig S47. MALDI-TOF spectrum of *L*-PLA obtained by reaction of *L*-LA and **1** in ratio 50:1 at 25 °C in CH_2Cl_2 (Bruker ultrafleXtreme; Polymerix – Sierra Analytics; Aachen).

Table S3. Polymerization data of *L*-LA using catalyst **1** on the variations of M_n with $[M]_0/[C]_0$ ratio in CH_2Cl_2 at 25 °C under argon atmosphere.

Entry	$[M]_0/[C]_0$	Time ^a (s)	Yield ^b (%)	$M_n^{(\text{obs})c}$ (kg/mol)	$M_n^{(\text{Theo})d}$ (kg/mol)	M_w/M_n	TOF ^e (h ⁻¹)
1	200:1	110	98	27.3	28.8	1.4	3200
2	400:1	190	99	49.1	57.5	1.5	3750
3	600:1	310	97	78.7	86.4	1.4	3370
4	800:1	425	98	104.0	115.3	1.4	3320
5	400 (400):1	175 (195)	95	98.4	115.3	1.4	3700

^aTime required for complete conversion. ^bIsolated yield of the polymer after quenching. ^cMeasured by GPC at 40 °C in THF, relative to polystyrene standards. ^d $M_n^{(\text{Theo})}$ at 100% conversion = $[M]_0/[C]_0 \times \text{mol. Wt. of monomer}$. ^eThe rate is expressed in terms of the turnover frequency (TOF), mol of LA consumed/(mol catalyst per h)) calculated with respect to number of Zn atom in the catalyst (monomeric structure in solution).

Calculation of Hydrodynamic Radii

To clarify whether the complexes are monomeric or dimeric in solution, diffusion-ordered spectroscopy (DOSY) NMR experiments in CDCl_3 were performed for complexes **1**, **3–6** and **8**, respectively. From the resulting diffusion coefficient values (D) of $1.21 \cdot 10^{-9}$ (**1**), $1.02 \cdot 10^{-9}$ (**3**), $9.58 \cdot 10^{-10}$ (**4**), $1.25 \cdot 10^{-9}$ (**5**), $1.25 \cdot 10^{-9}$ (**6**), and $1.13 \cdot 10^{-9} \text{ M}^2/\text{S}^2$ (**8**), respectively, we calculated the corresponding hydrodynamic radii (R_H) by using the Stokes-Einstein equation for a solute, $D = k_B T / (6\pi\eta R_H)$, where k_B is the Boltzmann constant, T the absolute temperature and η the fluid viscosity (η for CDCl_3 at 298 K is $0.55 \cdot 10^{-3} \text{ kg s}^{-1} \text{ m}^{-1}$).¹ The calculated R_H values of 3.33 (**1**), 3.95 (**3**), 4.21 (**4**), 3.22 (**5, 6**), and 3.57 Å (**8**), respectively, are very adjacent to half of the hydrodynamic radii of 6.51 (**1**), 7.97 (**3**), 6.34 (**4**), 6.75 (**6**) and 6.36 Å (**8**), respectively, which were calculated from the solid state structure. According to these studies, complexes **1–8** adopt mononuclear structures in CDCl_3 solution at ambient temperature.

Table S4 NBO analysis of the Zn atom and phenolic oxygen for compounds **1–8**

SL	Compound	NBO Charges of Zn atom Atomic unit (a.u.)	NBO Charges of Phenolic Oxygen Atomic unit (a.u.)
1	1	1.46	-0.98
2	2	1.44	-0.96
3	3	1.44	-0.96
4	4	1.44	-0.95
5	5	1.46	-0.97
6	6	1.44	-0.95
7	7	1.44	-0.95
8	8	1.44	-0.95

Computational details

DFT (*Density Functional Theory*) calculation of the mononuclear complexes were performed using the GAUSSIAN 16 (Rev A.03)¹ package of the quantum chemical programs at the B3LYP method, which is a version of the DFT method that uses the Becke's three parameter functional (B3) and includes a mixture of HF with DFT exchange terms associated with the gradient corrected correlation functional of the Lee, Yang and Parr (LYP) and LANL2DZ basis set.²

Reference

- [1] Gaussian 16, Revision A.03, M. J. Frisch, G. W. Trucks, H. B. Schlegel, G. E. Scuseria, M. A. Robb, J. R. Cheeseman, G. Scalmani, V. Barone, G. A. Petersson, H. Nakatsuji, X. Li, M. Caricato, A. V. Marenich, J. Bloino, B. G. Janesko, R. Gomperts, B. Mennucci, H. P. Hratchian, J. V. Ortiz, A. F. Izmaylov, J. L. Sonnenberg, D. Williams-Young, F. Ding, F. Lipparini, F. Egidi, J. Goings, B. Peng, A. Petrone, T. Henderson, D. Ranasinghe, V. G. Zakrzewski, J. Gao, N. Rega, G. Zheng, W. Liang, M. Hada, M. Ehara, K. Toyota, R. Fukuda, J. Hasegawa, M. Ishida, T. Nakajima, Y. Honda, O. Kitao, H. Nakai, T. Vreven, K. Throssell, J. A. Montgomery, Jr., J. E. Peralta, F. Ogliaro, M. J. Bearpark, J. J. Heyd, E. N. Brothers, K. N. Kudin, V. N. Staroverov, T. A. Keith, R. Kobayashi, J. Normand, K. Raghavachari, A. P. Rendell, J. C. Burant, S. S. Iyengar, J. Tomasi, M. Cossi, J. M. Millam, M. Klene, C. Adamo, R. Cammi, J. W. Ochterski, R. L. Martin, K. Morokuma, O. Farkas, J. B. Foresman, D. J. Fox, Gaussian, Inc., Wallingford CT, **2016**.
- [2] a) I. B. Obot, N. O. Obi-Egbedi, Corros. Sci. **2010**, *52*, 657–660; b) C. G. Zhan, J. A. Nicholes, D. A. Dixon, J. Phys. Chem. A **2003**, *107*, 4184–4195.